THE JOURNAL OF BIOLOGICAL CHEMISTRY
Vol. 278, No. 22, Issue of May 30, pp. 20245–20258, 2003

*Printed in U.S.A.*

# Importance of Conserved N-domain Residues Thr$^{441}$, Glu$^{442}$, Lys$^{515}$, Arg$^{560}$, and Leu$^{562}$ of Sarcoplasmic Reticulum $Ca^{2+}$-ATPase for MgATP Binding and Subsequent Catalytic Steps

PLASTICITY OF THE NUCLEOTIDE-BINDING SITE*

Received for publication, February 3, 2003
Published, JBC Papers in Press, March 20, 2003, DOI 10.1074/jbc.M301122200

**Johannes D. Clausen‡, David B. McIntosh§¶, Bente Vilsen‡, David G. Woolley§, and Jens Peter Andersen‡‖**

*From the ‡Department of Physiology, University of Aarhus, DK-8000 Aarhus C, Denmark and the §Division of Chemical Pathology, Department of Clinical Laboratory Sciences, Faculty of Health Sciences, University of Cape Town, Cape Town 7925, South Africa*

**Nine single mutations were introduced to amino acid residues Thr$^{441}$, Glu$^{442}$, Lys$^{515}$, Arg$^{560}$, Cys$^{561}$, and Leu$^{562}$ located in the nucleotide-binding domain of sarcoplasmic reticulum $Ca^{2+}$-ATPase, and the functional consequences were studied in a direct nucleotide binding assay, as well as by steady-state and transient kinetic measurements of the overall and partial reactions of the transport cycle. Some partial reaction steps were also examined in mutants with alterations to Phe$^{487}$, Arg$^{489}$, and Lys$^{492}$. The results implicate all these residues, except Cys$^{561}$, in high affinity nucleotide binding at the substrate site. Mutations Thr$^{441}$ → Ala, Glu$^{442}$ → Ala, and Leu$^{562}$ → Phe were more detrimental to MgATP binding than to ATP binding, thus pointing to a role for these residues in the binding of $Mg^{2+}$ or to a difference between the interactions with MgATP and ATP. Subsequent catalytic steps were also selectively affected by the mutations, showing the involvement of the nucleotide-binding domain in these reactions. Mutation of Arg$^{560}$ inhibited phosphoryl transfer but enhanced the $E_1PCa_2$ → $E_2P$ conformational transition, whereas mutations Thr$^{441}$ → Ala, Glu$^{442}$ → Ala, Lys$^{492}$ → Leu, and Lys$^{515}$ → Ala inhibited the $E_1PCa_2$ → $E_2P$ transition. Hydrolysis of the $E_2P$ phosphoenzyme intermediate was enhanced in Glu$^{442}$ → Ala, Lys$^{492}$ → Leu, Lys$^{515}$ → Ala, and Arg$^{560}$ → Glu. None of the mutations affected the low affinity activation by nucleotide of the phosphoenzyme-processing steps, indicating that modulatory nucleotide interacts differently from substrate nucleotide. Mutation Glu$^{442}$ → Ala greatly enhanced reaction of Lys$^{515}$ with fluorescein isothiocyanate, indicating that the two residues form a salt link in the native protein.**

The sarcoplasmic reticulum $Ca^{2+}$-ATPase[1] is an energy-transducing enzyme responsible for active transport of $Ca^{2+}$ from the cytosol into the lumen of sarcoplasmic reticulum. It is an integral 110-kDa membrane protein belonging to the family of P-type ATPases, in which autophosphorylation by ATP of a conserved aspartic acid residue is coupled to conformational changes resulting in ion translocation (Scheme 1). The high resolution x-ray structure of the $Ca^{2+}$-ATPase crystallized in a $Ca^{2+}$-bound dephospho form (presumably corresponding to $E_1Ca_2$ in Scheme 1) has revealed that the enzyme is made up of 10 membrane-spanning helices and a large cytoplasmic head that binds ATP and catalyzes its hydrolysis to yield ADP and $P_i$. The head consists of three well defined domains: the nucleotide-binding domain ("domain *N*," supposed to bind the adenosine part of ATP), phosphorylation domain ("domain *P*" with Asp$^{351}$, which is phosphorylated), and actuator domain ("domain *A*," believed to undergo large movements during the reaction cycle) (1). The catalytic site may, at different stages of the transport cycle, consist of residues contributed from all three head domains, and many questions regarding the nature of the nucleotide-binding site(s) are unresolved.

In domain *N*, labeling of Lys$^{515}$ with FITC (2, 3) or Lys$^{492}$ with TNP-8$N_3$-ATP (4) is competitive with respect to ATP binding at the catalytic site. The specific photolabeling of Lys$^{492}$ with TNP-8$N_3$-ATP has permitted measurement of the binding of nucleotide to mutant $Ca^{2+}$-ATPases in a competition assay and identified Phe$^{487}$, Arg$^{489}$, and Lys$^{492}$ as likely nucleotide-binding residues (5). The location of TNP-AMP in the crystal structure, obtained from a difference Fourier map following soaking of the $E_1Ca_2$ crystals in a solution containing TNP-AMP, supported involvement of these residues in the binding of nucleotide, and in addition revealed the proximity of TNP-AMP to several other residues, including Thr$^{441}$, Glu$^{442}$, Lys$^{515}$, Arg$^{560}$, and Leu$^{562}$ (1).

* This work was supported in part by grants from the Danish Medical Research Council, the Novo Nordisk Foundation, Denmark, the Lundbeck Foundation, Denmark, the Research Foundation of Aarhus University (to J. P. A. and B. V.), and the National Research Foundation of South Africa (to D. B. M.). The costs of publication of this article were defrayed in part by the payment of page charges. This article must therefore be hereby marked "*advertisement*" in accordance with 18 U.S.C. Section 1734 solely to indicate this fact.

¶ To whom correspondence may be addressed: Division of Chemical Pathology, Dept. of Clinical Laboratory Sciences, Faculty of Health Sciences, University of Cape Town, Cape Town 7925, South Africa. Fax: 27-21-4488150; E-mail: davidmci@chempath.uct.ac.za.

‖ To whom correspondence may be addressed: Dept. of Physiology, University of Aarhus, Ole Worms Allé 160, DK-8000 Aarhus C, Denmark. Fax: 45-86129065; E-mail: jpa@fi.au.dk.

[1] The abbreviations used are: $Ca^{2+}$-ATPase, the sarco(endo)plasmic reticulum $Ca^{2+}$-transporting adenosine triphosphatase (EC 3.6.1.38); CrATP, $\beta,\gamma$-bidentate chromium(III) complex of ATP; $E_1$, enzyme form with cytoplasmically facing high affinity $Ca^{2+}$-binding sites; $E_2$, enzyme form with low affinity for $Ca^{2+}$; $E_1PCa_2$, phosphoenzyme intermediate containing $Ca^{2+}$ in the occluded state; $E_2P$, phosphoenzyme intermediate with luminally facing low affinity $Ca^{2+}$-binding sites; EPPS, *N*-2-hydroxyethylpiperazine-*N*′-3-propanesulfonic acid; FITC, fluorescein isothiocyanate; MES, 2-(*N*-morpholino)ethanesulfonic acid; MOPS, 3-(*N*-morpholino)propanesulfonic acid; TES, *N*-tris(hydroxymethyl)-methyl-2-aminoethanesulfonic acid; TMAH, tetramethylammonium hydroxide; TNP-AMP, 2′,3′-*O*-(2,4,6-trinitrophenyl) adenosine 5′-monophosphate; TNP-8$N_3$-ATP, 2′,3′-*O*-(2,4,6-trinitrophenyl)-8-azido-adenosine 5′-triphosphate.

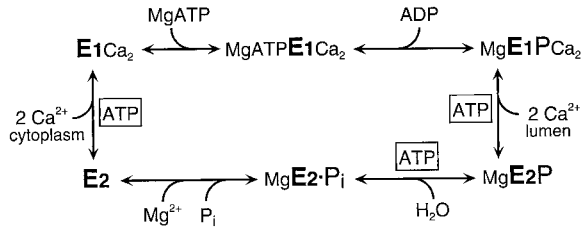


SCHEME 1. **$Ca^{2+}$-ATPase reaction cycle.** Major conformational changes and ligand binding and dissociation steps are shown. *Boxed ATP* indicates steps for which the rate is enhanced by additional binding of ATP or MgATP that is not hydrolyzed ("modulatory ATP").

A surprising feature of the crystal structure of the $Ca^{2+}$-bound $E_1Ca_2$ dephospho form is that the configuration of the cytoplasmic domains is quite open with the nucleotide-binding site being separated from $Asp^{351}$ in domain *P* by more than 25 Å, implying large domain movements during ATP binding and hydrolysis (1). Presumably, the binding of nucleotide leads to closing of the structure. The movements contribute to uncertainties about the nucleotide-binding residues and the orientation of the bound nucleotide. Although the high affinity binding sites for TNP-nucleotide and ATP seem to overlap (6), they are not necessarily identical. Thapsigargin, a potent inhibitor of the $Ca^{2+}$-ATPase, has no effect on TNP-ATP or TNP-8$N_3$-ATP binding, and yet decreases the affinity of the pump for ATP by at least 100-fold (5, 7). The doubts with respect to the nucleotide site are exacerbated by functional studies showing that ATP in addition to being the phosphorylating substrate exerts modulatory effects on various steps of the pump cycle, see *boxed* ATP in Scheme 1 (8–16). In view of the predicted large domain movements and presence of the phosphoryl group at the catalytic site during part of the cycle, it seems unlikely that modulatory ATP binds exactly as substrate ATP does.

In the present study, we have introduced mutations of $Thr^{441}$, $Glu^{442}$, $Lys^{515}$, $Arg^{560}$, $Cys^{561}$, and $Leu^{562}$, and we have also extended the previous study (5) on mutants with alterations to $Phe^{487}$, $Arg^{489}$, and $Lys^{492}$. With the exception of $Cys^{561}$, these residues show a high degree of conservation throughout the P-type ATPase family (17). A recent study, applying solution nuclear magnetic resonance techniques to a 28-kDa recombinant $Ca^{2+}$-ATPase fragment corresponding to domain *N* pinpointed $Thr^{441}$ and $Glu^{442}$ as the two residues providing the largest shifts in the backbone $^{15}N$ spectra upon addition of a non-hydrolyzable ATP analogue to the medium (18). Marked spectral shifts were also seen for residues close in the linear sequence to $Lys^{492}$, $Lys^{515}$, and $Arg^{560}$. Site-directed mutagenesis studies have previously shown the importance of $Lys^{515}$ and $Arg^{560}$ in the overall ATPase function (19–21). Mutation of $Lys^{515}$ to arginine, alanine, glutamine, and glutamate resulted in 65, 30, 25, and 5% $Ca^{2+}$-transport activity relative to wild type (19, 20). Mutation of $Arg^{560}$ to alanine abolished phosphorylation from ATP (21). $Thr^{441}$, $Glu^{442}$, $Cys^{561}$, and $Leu^{562}$, or their homologues in other P-type ATPases, have not been subjected previously to mutational analysis.

This study, presenting the first direct measurements of nucleotide-binding properties of mutants with alterations to $Thr^{441}$, $Glu^{442}$, $Lys^{515}$, $Arg^{560}$, $Cys^{561}$, and $Leu^{562}$ of the $Ca^{2+}$-ATPase, reveals marked effects on nucleotide binding to the substrate site of the dephosphoenzyme, except in the case of the $Cys^{561}$ mutants. Moreover, our analysis of other steps in the pump cycle (Scheme 1) demonstrates that phosphorylation, the $Ca^{2+}$-translocating $E_1PCa_2 \rightarrow E_2P$ conformational transition, as well as the hydrolysis of the $E_2P$ phosphoenzyme intermediate are affected to various extents by the mutations. The low affinity modulatory effects of ATP on the phosphoenzyme-processing steps are, however, not significantly affected. Finally, we provide functional evidence for close interaction between $Lys^{515}$ and $Glu^{442}$ in experiments demonstrating direct involvement of $Glu^{442}$ in the labeling reaction of $Lys^{515}$ with FITC.

## EXPERIMENTAL PROCEDURES

*Mutagenesis, Expression, and Assays of Overall Function*—Oligonucleotide-directed mutagenesis of cDNA encoding the rabbit fast twitch muscle $Ca^{2+}$-ATPase (SERCA1a isoform) was carried out as described previously (22). For expression, the wild-type or mutant cDNA, inserted in the pMT2 vector (23), was transfected into COS-1 cells using the calcium phosphate precipitation method (24). The microsomal fraction containing expressed wild-type or mutant $Ca^{2+}$-ATPase was isolated by differential centrifugation (19). The concentration of expressed $Ca^{2+}$-ATPase was quantified by a specific enzyme-linked immunosorbent assay (25) or by determination of the maximum capacity for phosphorylation by inorganic phosphate in the presence of 30% (v/v) dimethyl sulfoxide ("active site concentration," see Ref. 26). Transport of $^{45}Ca^{2+}$ into the microsomal vesicles was measured by filtration, and the ATPase activity was measured by determining the amount of $P_i$ liberated as described previously (26).

*Phosphorylation from [γ-$^{32}$P]ATP and $^{32}P_i$*—Manual mixing experiments at various buffer and temperature conditions (detailed in the figure legends) were carried out according to the principles described previously (22, 25, 26). Transient kinetic experiments at 25 °C were performed using a Bio-Logic quench-flow module QFM-5 (Bio-Logic Science Instruments, Claix, France) as described (27). In all phosphorylation experiments, acid quenching was performed with 0.5–2 volumes of 25% (w/v) trichloroacetic acid containing 100 mM $H_3PO_4$. The acid-precipitated protein was washed by centrifugation and subjected to SDS-PAGE in a 7% polyacrylamide gel at pH 6.0 (28), and the radioactivity associated with the separated $Ca^{2+}$-ATPase band was quantified by imaging, using a Packard Cyclone™ Storage Phosphor System. Background phosphorylation levels, subtracted from all data points, were usually determined in parallel experiments with control microsomes isolated from mock-transfected COS-1 cells. In some of the dephosphorylation experiments, the constant phosphorylation level reached after the exponential decay was taken as background (usually ~5% of the initial phosphorylation).

To remove contaminant ADP and AMP, the non-radioactive ATP added in millimolar concentration in dephosphorylation experiments was purified by ion exchange chromatography on a Sephadex DEAE-A25 column before use. By using an NADH-coupled spectrophotometric assay with phosphoenolpyruvate, lactate dehydrogenase, and pyruvate kinase, the purified ATP preparation was found to contain less ADP than the detection limit of 0.1 mol %.

*Assays for Nucleotide Binding*—The synthesis of [γ-$^{32}$P]TNP-8$N_3$-ATP, the photolabeling of COS-1 cell microsomes containing wild-type or mutant $Ca^{2+}$-ATPase, the inhibition by ATP, and the quantification of labeled bands by electronic autoradiography following SDS-PAGE were carried out as described previously (5, 29). Generally, the concentration of [γ-$^{32}$P]TNP-8$N_3$-ATP was 3× $K_{0.5}$ in the inhibition experiments with ATP (where $K_{0.5}$ is ligand concentration giving half-maximum effect). Details of the buffer composition are given in the legends. CrATP-induced $Ca^{2+}$ occlusion was measured as described previously (5, 30).

*Calculations and Data Analysis*—The ion concentrations in the reaction buffers were calculated using the program WEBMAXC, available on the World Wide Web, and the stability constants therein (31). Generally, experiments were conducted at least twice, and the complete set of data was analyzed by nonlinear regression using the SigmaPlot program (SPSS, Inc.). Monoexponential functions were fitted to the phosphorylation and dephosphorylation time courses. The analysis of ligand concentration dependences was based on the Hill equation,

$$[EL] = E_{tot} \cdot [L]^n/(K_{0.5}{}^n + [L]^n) \quad \text{(Eq. 1)}$$

For analysis of the [γ-$^{32}$P]TNP-8$N_3$-ATP labeling data, a constant or linear component was added to represent nonspecific labeling as described (5), and the Hill coefficient was set to 1. The "true" dissociation constant for ATP and MgATP binding was calculated using the previously validated equation for competitive inhibition of the [γ-$^{32}$P]TNP-8$N_3$-ATP labeling (5).

## RESULTS

*Mutagenesis and Expression*—Nine $Ca^{2+}$-ATPase constructs with mutations of potential nucleotide-binding residues were

prepared in this study. $Thr^{441}$, $Glu^{442}$, and $Lys^{515}$ were replaced individually with alanine. $Cys^{561}$ was replaced with alanine or tryptophan; $Arg^{560}$ was replaced with leucine, valine, or glutamate; and $Leu^{562}$ was replaced with phenylalanine. The latter substitution was chosen to test the importance of the leucine for nucleotide binding by either introducing steric hindrance at this position or possibly enhancing the affinity for nucleotide by creating an aromatic "sandwich" for the adenine ring with $Phe^{487}$. All mutants could be expressed in COS-1 cells at levels similar to that of the wild type (data not shown), allowing studies of the overall function as well as the partial reactions of the enzyme cycle. In addition, some supplementary studies of partial reactions were carried out with previously constructed mutants (5) with alterations to $Phe^{487}$, $Arg^{489}$, and $Lys^{492}$.

*Overview of Functional Effects*—Fig. 1*A* shows ATP-driven $^{45}Ca^{2+}$ accumulation in microsomal vesicles measured in the presence of oxalate to trap $Ca^{2+}$ in the lumen. The MgATP concentration was 5 mM, *i.e.* several hundredfold higher than required to saturate the phosphorylation reaction in wild type. All the mutants were able to transport $Ca^{2+}$, albeit at reduced rates compared with wild type. The most significant reduction was seen for mutant $Arg^{560} \rightarrow$ Glu with a $Ca^{2+}$ transport rate corresponding to 17% that of the wild type, whereas ~80% transport was obtained for the $Cys^{561}$ mutants. The $Ca^{2+}$ transport rates of the remaining six mutants were roughly half (39–66%) that of wild type.

Fig. 1*B* shows the ATPase activity in the presence of 5 mM MgATP without oxalate, in the absence and presence of the calcium ionophore A23187. In the absence of ionophore (conditions resulting in net $Ca^{2+}$ uptake in the vesicles), a similar pattern was obtained for ATP hydrolysis as for $Ca^{2+}$ transport (Fig. 1*B*, *black columns*), $Arg^{560} \rightarrow$ Glu showing the most marked reduction of turnover rate, the $Cys^{561}$ mutants being wild type like, and the remaining six mutants hydrolyzing ATP at turnover rates of 40–58% as compared with wild type. The good correlation between the turnover rate for ATP hydrolysis and ATP-driven accumulation of $Ca^{2+}$ in the microsomes demonstrates that the coupling between ATP hydrolysis and $Ca^{2+}$ transport was retained in the mutants. Addition of calcium ionophore A23187 to the reaction medium increased the rate of ATP hydrolysis in the wild type 2–3-fold because of relief of the "back inhibition" of the rate-limiting $E_1PCa_2 \rightarrow E_2P$ transition imposed by $Ca^{2+}$ accumulated at high concentrations in the microsomal vesicles. A similar increase was seen for $Thr^{441} \rightarrow$ Ala, $Glu^{442} \rightarrow$ Ala, $Lys^{515} \rightarrow$ Ala, and the $Cys^{561}$ mutants, whereas for $Leu^{562} \rightarrow$ Phe and the three $Arg^{560}$ mutants the ATPase activity remained essentially unaltered (Fig. 1*B*, *gray columns*). The latter result implies that a reaction step other than the $E_1PCa_2 \rightarrow E_2P$ transition is rate-limiting in the case of $Leu^{562} \rightarrow$ Phe and $Arg^{560}$ mutants.

In the $Ca^{2+}$-bound $E_1Ca_2$ state, the wild-type $Ca^{2+}$-ATPase forms a phosphoenzyme intermediate by reaction with MgATP (*cf.* Scheme 1). Fig. 1*C* shows the results of experiments where phosphorylation of $Ca^{2+}$-saturated enzyme was carried out for 5 s at 25 °C with either 5 or 50 μM [γ-$^{32}$P]MgATP. For wild type, the maximum steady-state phosphoenzyme level of ~80% of the total active-site concentration is close to being reached at 5 μM MgATP; also for the $Cys^{561}$ mutants, there was not much difference between 5 and 50 μM MgATP. By contrast, mutants $Thr^{441} \rightarrow$ Ala, $Glu^{442} \rightarrow$ Ala, $Lys^{515} \rightarrow$ Ala, and in particular $Arg^{560} \rightarrow$ Leu, $Arg^{560} \rightarrow$ Val, and $Leu^{562} \rightarrow$ Phe showed much lower phosphoenzyme levels with 5 μM MgATP than with 50 μM MgATP, indicating a markedly reduced apparent affinity for the nucleotide, relative to wild type. Mutant $Arg^{560} \rightarrow$ Glu was unable to phosphorylate significantly above the background level at either concentration of MgATP (Fig. 1*C*).

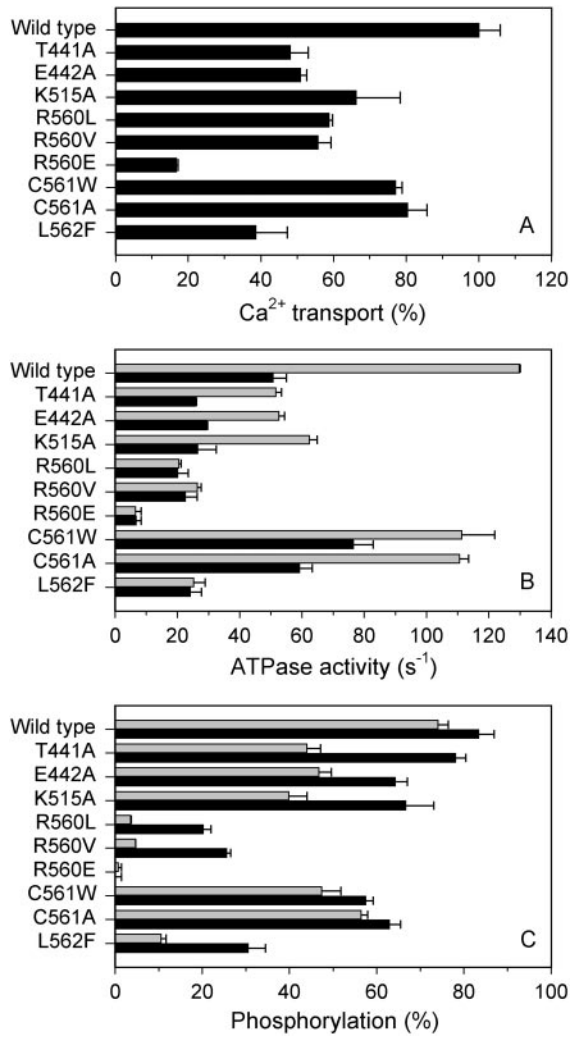


FIG. 1. **Initial overview of ATP-driven $Ca^{2+}$ transport (*A*), ATPase activity (*B*), and phosphorylation from ATP (*C*).** *A*, measurements of ATP-driven $Ca^{2+}$ transport were performed by filtration following incubation for 5 min at 37 °C in a medium containing 20 mM MOPS/Tris (pH 6.8), 100 mM KCl, 5 mM MgATP, 5 mM potassium oxalate (included to trap $Ca^{2+}$ inside the microsomal vesicles), 0.5 mM EGTA, and 0.45 mM $^{45}CaCl_2$. The $Ca^{2+}$ transport activity of the wild type was taken as 100%, and each mutant was related to this level following correction for the variation in expression level. *B*, the rate of $Ca^{2+}$-activated ATP hydrolysis was determined at 37 °C in the presence (*gray bars*) or absence (*black bars*) of 1 μM $Ca^{2+}$ ionophore A23187 in a medium containing 50 mM TES/Tris (pH 7.0), 100 mM KCl, 7 mM $MgCl_2$, 1 mM EGTA, 0.9 mM $CaCl_2$ (giving a free $Ca^{2+}$ concentration of 3 μM), and 5 mM ATP. Following subtraction of the background activity determined in the absence of $Ca^{2+}$, the molecular activity (catalytic turnover rate) shown was calculated as the amount of $P_i$ liberated per $Ca^{2+}$-ATPase molecule/s. *C*, the phosphorylation with [γ-$^{32}$P]ATP was carried out for 5 s at 25 °C in a medium containing 40 mM MOPS/Tris (pH 7.0), 80 mM KCl, 5 mM $MgCl_2$, 100 μM $CaCl_2$, and either 5 μM [γ-$^{32}$P]ATP (*gray bars*) or 50 μM [γ-$^{32}$P]ATP (*black bars*). The phosphorylation level of the wild type incubated in a medium containing 100 mM MES/Tris (pH 6.0), 10 mM $MgCl_2$, 2 mM EGTA, 30% (v/v) dimethyl sulfoxide, and 0.5 mM $^{32}P_i$ for 10 min at 25 °C was taken as 100% ("active site concentration"), and all other values were related to this level following correction for the variation in expression level. Standard errors are indicated by the *error bars* on the *columns*.

*MgATP Dependence and Time Course of Phosphorylation from [γ-$^{32}$P]ATP*—The MgATP concentration dependence of phosphorylation was further investigated at 0 °C, where the ATP hydrolysis rate was sufficiently low to allow the phosphorylation to be studied at submicromolar concentrations of the substrate. As seen in Fig. 2*A*, a 10–120-fold reduction of apparent affinity for MgATP (increase of $K_{0.5}$) relative to

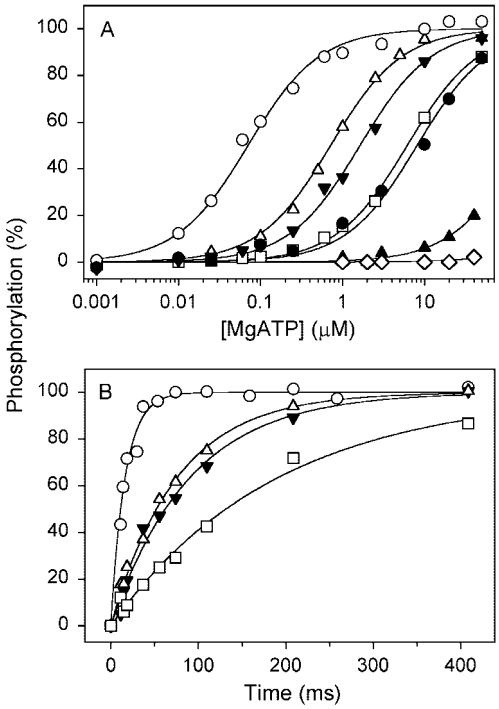


FIG. 2. **MgATP concentration dependence (*A*) and time course (*B*) of phosphorylation from ATP.** *A*, wild type and mutants were phosphorylated at 0 °C for 15 s in a medium containing 40 mM MOPS/Tris (pH 7.0), 80 mM KCl, 5 mM $MgCl_2$, 100 μM $CaCl_2$, and varying concentrations of [γ-$^{32}$P]ATP as indicated. The *lines* show the best fits of the Hill equation with the Hill coefficient set to 1, giving the $K_{0.5}$ values (in μM ± S.E.) indicated in parentheses: *open circles*, wild type, (0.067 ± 0.005); *open squares*, $Thr^{441} \rightarrow Ala$ (6.2 ± 0.6); *open triangles*, $Glu^{442} \rightarrow Ala$ (0.72 ± 0.06); *reversed solid triangles*, $Lys^{515} \rightarrow Ala$ (1.6 ± 0.2); *open diamonds*, $Arg^{560} \rightarrow Leu$ (≫100); *solid triangles*, $Arg^{560} \rightarrow Val$ (~100); and *solid circles*, $Leu^{562} \rightarrow Phe$ (8.1 ± 1.4). The 100% value corresponds to the phosphorylation level reached at infinite ATP concentration as deduced from the fit. *B*, phosphorylation was carried out at 25 °C in a medium containing 40 mM MOPS/Tris (pH 7.0), 80 mM KCl, 100 μM $CaCl_2$, 5 mM $MgCl_2$, and 5 μM [γ-$^{32}$P]ATP, and the samples were acid-quenched at serial time intervals, using a Bio-Logic QFM-5 quench-flow module with mixing protocol as described previously (34). In each case, the level of phosphorylation after 5 s was taken as 100% (for a comparison of the specific phosphorylation levels of wild type and mutants after 5 s, see Fig. 1*C*). The *lines* show the best fits of a monoexponential function, giving the rate constants (in $s^{-1}$ ± S.E.) indicated in *parentheses*: *open circles*, wild type (59.7 ± 2.0); *open squares*, $Thr^{441} \rightarrow Ala$ (5.3 ± 0.6); *open triangles*, $Glu^{442} \rightarrow Ala$ (13.3 ± 0.6); *reversed solid triangles*, $Lys^{515} \rightarrow Ala$ (11.1 ± 0.8).

wild type was found for mutants $Thr^{441} \rightarrow Ala$, $Glu^{442} \rightarrow Ala$, $Lys^{515} \rightarrow Ala$, and $Leu^{562} \rightarrow Phe$; and for mutants $Arg^{560} \rightarrow Leu$ and $Arg^{560} \rightarrow Val$, the $K_{0.5}$ for MgATP was at least 3 orders of magnitude lower than that of wild type.

Fig. 2*B* shows the time course of phosphorylation at 25 °C of wild type and selected mutants determined by quench-flow methodology in the presence of 5 μM [γ-$^{32}$P]MgATP under conditions identical to those corresponding to Fig. 1*C*. $Leu^{562} \rightarrow Phe$ and the three $Arg^{560}$ mutants were not included in these studies because their phosphorylation levels were too low to allow reliable pre-steady-state measurements (*cf.* Fig. 1*C*). The wild type reaches a steady-state level of phosphorylation within a few hundred milliseconds, with a slight initial overshoot (Fig. 2*B*, *cf.* also Ref. 27). For simplicity, a monoexponential function was fitted to the data, giving an apparent rate constant $k_{obs}$ = 60 $s^{-1}$ for the approach to steady state. In comparison, 5–12-fold lower $k_{obs}$ values were determined for mutants $Thr^{441} \rightarrow Ala$, $Glu^{442} \rightarrow Ala$, and $Lys^{515} \rightarrow Ala$ (Fig. 2*B*). The $k_{obs}$ value decreased in the same order as the apparent

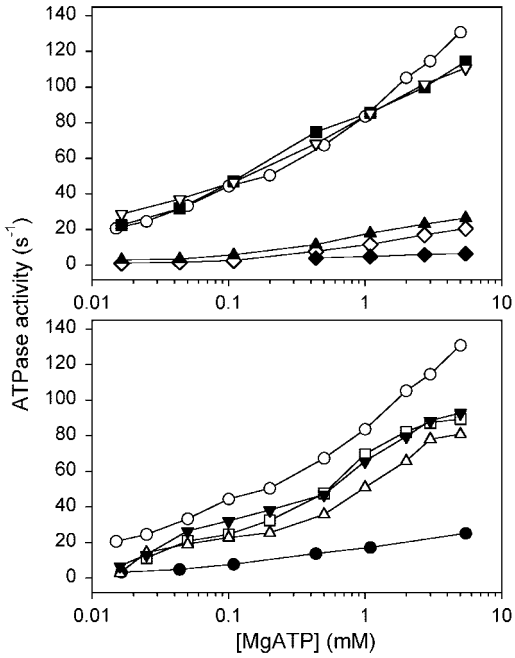


FIG. 3. **MgATP dependence of ATPase activity.** The rate of ATP hydrolysis was measured at 37 °C in a medium containing 50 mM TES/Tris (pH 7.5), 100 mM KCl, 100 μM $CaCl_2$, 1 μM $Ca^{2+}$ ionophore A23187, and varying concentrations of $Mg^{2+}$ and ATP to give the indicated MgATP concentrations and 1 mM free $Mg^{2+}$. Following subtraction of the background activity determined in the absence of $Ca^{2+}$ (presence of 1 mM EGTA without $CaCl_2$), the catalytic turnover rate shown was calculated as the amount of $P_i$ liberated per $Ca^{2+}$-ATPase molecule/s. The symbols are as follows: *open circles*, wild type; *reversed open triangles*, $Cys^{561} \rightarrow Ala$; *solid squares*, $Cys^{561} \rightarrow Trp$; *solid triangles*, $Arg^{560} \rightarrow Val$; *open diamonds*, $Arg^{560} \rightarrow Leu$; *solid diamonds*, $Arg^{560} \rightarrow Glu$; *open squares*, $Thr^{441} \rightarrow Ala$; *open triangles*, $Glu^{442} \rightarrow Ala$; *reversed solid triangles*, $Lys^{515} \rightarrow Ala$ and *solid circles*, $Leu^{562} \rightarrow Phe$.

MgATP affinity observed in Fig. 2*A* ($Glu^{442} \rightarrow Ala > Lys^{515} \rightarrow Ala > Thr^{441} \rightarrow Ala$).

*MgATP Dependence of ATP Hydrolysis*—For wild-type $Ca^{2+}$-ATPase, the MgATP activation profile of ATPase activity has a complex appearance, because MgATP (or ATP) in addition to being the phosphorylating substrate exerts modulatory effects on various steps of the pump cycle, *cf.* Scheme 1 (8–16). The basal activation to about 20% of the maximum activity occurring at MgATP concentrations below 10 μM in wild type reflects the binding of MgATP to the $E_1Ca_2$ form as phosphorylating substrate. It can be seen in Fig. 3 that for mutant $Leu^{562} \rightarrow Phe$ and the three $Arg^{560}$ mutants, the basal activation was shifted to much higher MgATP concentrations in agreement with the data in Fig. 2*A*. Less drastic right-shifts of the basal activation were observed for mutants $Thr^{441} \rightarrow Ala$, $Glu^{442} \rightarrow Ala$, and $Lys^{515} \rightarrow Ala$ with plateau levels being reached at about 50 μM MgATP, whereas the $Cys^{561}$ mutants were wild type-like. At least two secondary activation phases occur for the wild-type enzyme, between 10 and 200 μM MgATP and at higher MgATP concentrations, reflecting the accelerating effect of nucleotide on partial reaction steps preceding and subsequent to phosphorylation (9, 10, 12–16). Fig. 3 shows that the $Cys^{561}$ mutants displayed a wild type-like secondary activation. For mutant $Leu^{562} \rightarrow Phe$ and the three $Arg^{560}$ mutants, the severely reduced ATPase activity prevented a clear distinction between the basal and the intermediate modulatory phases (Fig. 3), but a distinct low affinity activation phase similar to that of the wild type is seen above 200 μM MgATP for $Arg^{560} \rightarrow Leu$, $Arg^{560} \rightarrow Val$, and $Leu^{562} \rightarrow Phe$, as well as for $Thr^{441} \rightarrow Ala$, $Glu^{442} \rightarrow Ala$, and $Lys^{515} \rightarrow Ala$, indicating that nucleotide binding with low affinity accelerates at least one partial reac-

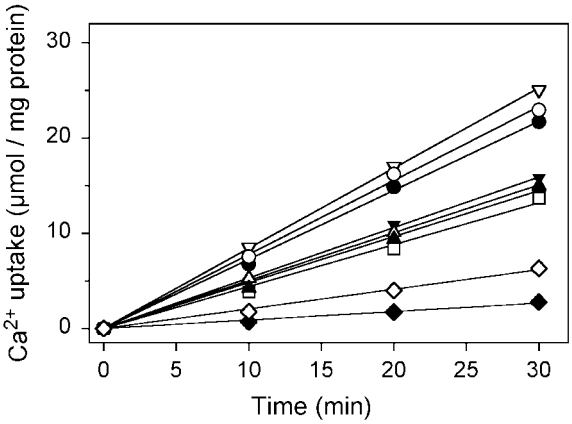


FIG. 4. **Acetyl phosphate-driven $Ca^{2+}$ transport.** Transport activity of COS-1 cell microsomes was measured at 25 °C in 25 mM MOPS/Tris (pH 6.8), 100 mM KCl, 5 mM $MgCl_2$, 0.55 mM $^{45}CaCl_2$, 0.5 mM EGTA, 5 mM potassium oxalate, and 10 mM acetyl phosphate for the times shown. The *ordinate* shows the amount of $Ca^{2+}$ accumulated per mg of $Ca^{2+}$-ATPase protein. The symbols are as follows: *open circles*, wild type; *open squares* $Thr^{441} \rightarrow Ala$; *open triangles*, $Glu^{442} \rightarrow Ala$; *reversed solid triangles*, $Lys^{515} \rightarrow Ala$; *solid triangles*, $Arg^{560} \rightarrow Val$; *open diamonds*, $Arg^{560} \rightarrow Leu$; *solid diamonds*, $Arg^{560} \rightarrow Glu$; *reversed open triangles,* $Cys^{561} \rightarrow Ala$; and *solid circles*, $Leu^{562} \rightarrow Phe$.

tion in these mutants, although in contrast to the wild type the activation profiles level off above 3 mM MgATP for $Thr^{441} \rightarrow Ala$, $Glu^{442} \rightarrow Ala$, and $Lys^{515} \rightarrow Ala$. Furthermore, taking into consideration that the basal activation is shifted to higher MgATP concentrations relative to wild type, the activation occurring with intermediate affinity, between 10 and 200 $\mu$M MgATP in wild type, seems to be less pronounced or right-shifted in $Thr^{441} \rightarrow Ala$, $Glu^{442} \rightarrow Ala$, and $Lys^{515} \rightarrow Ala$. This is most obvious for $Glu^{442} \rightarrow Ala$, where the ATPase activity was nearly constant between 50 and 200 $\mu$M MgATP (Fig. 3).

*Acetyl Phosphate-driven $Ca^{2+}$ Uptake*—As an alternative to ATP, acetyl phosphate can be used as an energy source to drive $Ca^{2+}$ transport into the microsomal vesicles (16). Fig. 4 shows the time course for wild type and the mutants. For most mutants, the decrease of the transport rate relative to wild type was rather similar to the decrease seen for ATP-driven transport at 5 mM MgATP (Fig. 1*A*), as also shown previously for mutant $Lys^{515} \rightarrow Ala$ (20), indicating that at high MgATP concentration (Fig. 1, *A* and *B*) the limitation of the overall reaction rate seen for the mutants is not imposed by binding defects specific to the nucleotide, but rather by defects in other partial reaction steps. Interestingly, mutant $Leu^{562} \rightarrow Phe$ is a clear exception to this pattern. This mutant showed a markedly reduced ATP-driven $Ca^{2+}$ transport (Fig. 1*A*) and ATPase activity (Fig. 1*B*), but wild type-like acetyl phosphate-dependent $Ca^{2+}$ transport (Fig. 4).

*$Ca^{2+}$ Dependence*—To examine whether a reduced affinity for $Ca^{2+}$ could be involved in the observed effects of the mutations on $Ca^{2+}$ transport and ATPase activity, we performed a $Ca^{2+}$ titration of the ATPase activity. The $Ca^{2+}$ concentration giving half-maximum activation of ATP hydrolysis was 0.33 ± 0.01 $\mu$M for the wild type and 0.64 ± 0.05, 0.41 ± 0.02, 0.35 ± 0.02, 0.33 ± 0.02, 0.54 ± 0.04, 0.38 ± 0.02, 0.47 ± 0.04, and 0.38 ± 0.03 $\mu$M for $Arg^{560} \rightarrow Leu$, $Arg^{560} \rightarrow Val$, $Cys^{561} \rightarrow Ala$, $Cys^{561} \rightarrow Trp$, $Leu^{562} \rightarrow Phe$, $Thr^{441} \rightarrow Ala$, $Glu^{442} \rightarrow Ala$, and $Lys^{515} \rightarrow Ala$, respectively (the $K_{0.5}$ value was obtained by fitting the Hill equation, ± S.E., from the regression analysis, data not shown). Thus, although significant alterations to $Ca^{2+}$ binding are evident for mutants $Arg^{560} \rightarrow Leu$ and $Leu^{562} \rightarrow Phe$, the mutants were >80% saturated with $Ca^{2+}$ at the free $Ca^{2+}$ concentration of 3 $\mu$M present during the experiments corresponding to Fig. 1, *A* and *B*, and close to 100% saturated at the higher free $Ca^{2+}$ concentrations present during the experiments corresponding to Fig. 1*C*, Fig. 2, *A* and *B*, Fig. 3, and Fig. 4. Hence, the observed effects of the mutations cannot be ascribed to variable $Ca^{2+}$ saturation.

*Nucleotide Binding*—To examine the mutational effects on nucleotide binding directly, we applied a photolabeling assay that takes advantage of the highly specific labeling of $Lys^{492}$ with [$\gamma$-$^{32}$P]TNP-8$N_3$-ATP (5). In this assay, the affinities for the free and $Mg^{2+}$-bound forms of [$\gamma$-$^{32}$P]TNP-8$N_3$-ATP are determined from the dependence of photolabeling on the concentration of the label in the absence and presence of $Mg^{2+}$, respectively. By studying competitive inhibition of photolabeling in the presence of varying concentrations of ATP and MgATP (the latter often being referred to as the "true" substrate (32)), it is also possible to obtain highly accurate values for the $K_D$ corresponding to these nucleotides (5, 33, 34). Photolabeling is carried out in the absence of $Ca^{2+}$ to avoid phosphorylation of the $Ca^{2+}$-ATPase and hydrolysis of the photolabel, and at pH 8.5 to reduce nonspecific labeling and ensure that the predominant enzyme conformation is $E_1$ (5). Results of photolabeling experiments with the nine mutants in the absence and presence of $Mg^{2+}$ are summarized in Table I. Also presented here for the first time are nucleotide-binding parameters in the absence of $Mg^{2+}$ for mutants $Phe^{487} \rightarrow Leu$, $Arg^{489} \rightarrow Leu$, and $Lys^{492} \rightarrow Tyr$ of the $^{487}$FSRDRK loop in domain *N*. These latter mutants have only been analyzed previously in the presence of $Mg^{2+}$ (5). We have shown before (33, 34), and reproduced in Table I, that wild type exhibits a striking $Mg^{2+}$ dependence for both TNP-8$N_3$-ATP and ATP binding; $Mg^{2+}$ lowers the apparent affinity for the TNP-nucleotide and increases (as much as 40-fold) that for ATP.

The two $Cys^{561}$ mutants differed little from wild type in the binding assays, whereas the remaining mutants showed interesting differences from wild type (Table I). Examining the interaction with TNP-8$N_3$-ATP and TNP-8$N_3$-MgATP first, there were major changes relative to wild type in both labeling efficiency and in the apparent affinity for the photolabel. $Lys^{515} \rightarrow Ala$ and $Arg^{560} \rightarrow Glu$ showed no specific photolabeling above the background level either in the absence or presence of $Mg^{2+}$, and $Arg^{560} \rightarrow Val$ could not be labeled in the absence of $Mg^{2+}$. $Arg^{560} \rightarrow Leu$ and $Arg^{560} \rightarrow Val$ showed conspicuous ~10-fold decreases, relative to wild type, of the apparent affinity for the photolabel (*i.e.* increased $K_{0.5}$) in the presence of $Mg^2$, whereas $Thr^{441} \rightarrow Ala$, $Glu^{442} \rightarrow Ala$, and $Leu^{562} \rightarrow Phe$ showed slight increases of the apparent affinity (*i.e.* reduced $K_{0.5}$). It is evident that $Arg^{560}$ plays a major role in binding the TNP-nucleotide in the presence of $Mg^{2+}$. On the other hand, $Arg^{560} \rightarrow Leu$ showed no significant deviation from wild type in the absence of $Mg^{2+}$. In $Thr^{441} \rightarrow Ala$, the ability to respond to $Mg^{2+}$ with a reduced affinity for the TNP-nucleotide was lost; in the presence of $Mg^{2+}$ this mutant displayed an affinity for the photolabel similar to or slightly higher than that displayed in the absence of $Mg^{2+}$, whereas in the wild type $Mg^{2+}$ reduces the affinity for the photolabel. With respect to the three mutants with alterations to residues of the $^{487}$FSRDRK loop, $Arg^{489} \rightarrow Leu$ and $Lys^{492} \rightarrow Tyr$ showed a large decrease in affinity for the photolabel relative to wild type in the absence of $Mg^{2+}$, corresponding to 31- and 17-fold, respectively, whereas $Phe^{487} \rightarrow Leu$ exhibited an increased affinity. Evidently the two basic amino acid residues are critical for binding the nucleotide in the absence of $Mg^{2+}$.

Although the binding sites for ATP and TNP-8$N_3$-ATP may not be identical, there is sufficient overlap to ensure efficient competition when ATP or MgATP is added at varying concentrations during photolabeling, and we have previously demonstrated that the competition assay provides highly accurate

TABLE I
*Nucleotide binding parameters in the presence and absence of $Mg^{2+}$*

Photolabeling with [$\gamma$-$^{32}$P]TNP-8$N_3$-ATP was carried out as described in Ref. 5 and competition with ATP/MgATP as described in Ref. 5 and illustrated in Fig. 5. The parameters shown were derived from analysis of the data as described for Fig. 5 and under "Experimental Procedures."

| | $Mg^{2+}$/EGTA[a] | | | EDTA[b] | | |
|---|---|---|---|---|---|---|
| | $K_{0.5}$ (TNP-8$N_3$-MgATP) | $K_D$ (MgATP)[c] | $K_D$ (MgADP)[c] | $K_{0.5}$ (TNP-8$N_3$-ATP) | $K_D$ (ATP)[c] | $K_D$ (ADP)[c] |
| | | $\mu$M | | | $\mu$M | |
| Wild type | 0.79 | 0.51 | 3.7 | 0.20 | 21 | 28 |
| Thr$^{441}$ → Ala | 0.22 | 62 | 104 | 0.31 | 73 | 221 |
| Glu$^{442}$ → Ala | 0.46 | 92 | | 0.090 | 100 | |
| Lys$^{515}$ → Ala | | | No specific labeling | | | |
| Arg$^{560}$ → Leu | 9.9 | 880 | 700 | 0.26 | 630 | >2500 |
| Arg$^{560}$ → Val | 7.8 | 21 | | | No specific labeling | |
| Arg$^{560}$ → Glu | | | No specific labeling | | | |
| Cys$^{561}$ → Ala | 0.52 | 0.98 | | 0.18 | 16 | |
| Cys$^{561}$ → Trp | 1.0 | 1.3 | | 0.22 | 18 | |
| Leu$^{562}$ → Phe | 0.20 | 35 | | 0.093 | 43 | |
| Phe$^{487}$ → Leu | 0.34[d] | 11[d] | | 0.040 | 250 | |
| Arg$^{489}$ → Leu | 0.67[d] | 8.1[d] | | 6.2 | >1000 | |
| Lys$^{492}$ → Tyr | 0.28[d] | 49[d] | | 3.4 | >1000 | |

[a] Medium: 25 mM EPPS/TMAH (pH 8.5), 20% (v/v) glycerol, 1 mM $MgCl_2$, 0.5 mM EGTA.
[b] Medium: 25 mM EPPS/TMAH (pH 8.5), 20% (v/v) glycerol, 2 mM EDTA.
[c] The "true" $K_D$ calculated from the measured $K_{0.5}$ values under the assumption of competitive inhibition as described previously (5). In the inhibition experiments, the concentration of [$\gamma$-$^{32}$P]TNP-8$N_3$-ATP was 3 × $K_{0.5}$, except for mutants Arg$^{560}$ → Leu and Arg$^{560}$ → Val in the presence of $Mg^{2+}$ and EGTA, and Arg$^{489}$ → Leu in the presence of EDTA, where it was equal to the $K_{0.5}$.
[d] Data from Ref. 5 included for comparison.

values for the ATP and MgATP binding affinities of wild type and mutant $Ca^{2+}$-ATPases expressed in COS-1 cells (5). For wild type, the true affinities ($K_D$ values) for MgATP and ATP calculated under the assumption of competitive inhibition as described previously (5) were found to be 0.51 and 21 $\mu$M, respectively (Table I). Fig. 5 shows examples of the experimental data from which the $K_D$ values for ATP and MgATP in Table I were derived, corresponding to Thr$^{441}$ → Ala, Glu$^{442}$ → Ala, Arg$^{560}$ → Leu, and Leu$^{562}$ → Phe, with data for wild type (see also Refs. 5 and 33) indicated by *dashed lines without data points*. Because of the deficient photolabeling described above, competition experiments could not be carried out for Lys$^{515}$ → Ala and Arg$^{560}$ → Glu. Mutation Arg$^{560}$ → Leu decreased the affinity (*i.e.* increased $K_D$) for MgATP more than 1000-fold, whereas mutations Cys$^{561}$ → Ala and Cys$^{561}$ → Trp had little effect, as mentioned above. A decrease of affinity for MgATP of 40-fold relative to wild type was seen for Arg$^{560}$ → Val, and as much as 70–180-fold for Thr$^{441}$ → Ala, Glu$^{442}$ → Ala, and Leu$^{562}$ → Phe. In the absence of $Mg^{2+}$, Arg$^{560}$ → Leu still showed a conspicuous 30-fold decrease of affinity for ATP, whereas for Thr$^{441}$ → Ala, Glu$^{442}$ → Ala, and Leu$^{562}$ → Phe, the affinity for ATP was only 2–5-fold reduced relative to wild type.

In the case of the $^{487}$FSRDRK mutants, Arg$^{489}$ → Leu and Lys$^{492}$ → Tyr showed extremely poor binding of ATP in the absence of $Mg^{2+}$, reproducing what was found for the TNP-nucleotide. For Phe$^{487}$ → Leu the changes in the presence and absence of $Mg^{2+}$ were rather similar, 10–20-fold reduced affinity compared with wild type.

For Thr$^{441}$ → Ala and Arg$^{560}$ → Leu, competition studies were also carried out with ADP. For wild type, the $K_D$ values for ADP in the presence and absence of $Mg^{2+}$ were 4 and 28 $\mu$M, respectively. For both Thr$^{441}$ → Ala and Arg$^{560}$ → Leu, there were pronounced decreases in affinity for ADP as well as MgADP (8- and >100-fold, respectively, for ADP, and ~30- and ~200-fold, respectively, for MgADP).

*CrATP-induced $Ca^{2+}$ Occlusion*—The conspicuous effects found in the above-described experiments testing the nucleotide-binding properties of the mutants, and the uncertainty with respect to Lys$^{515}$ → Ala, because it could not be photolabeled with TNP-8$N_3$-ATP, encouraged us to study, as an alternative, the binding of another nucleotide, the non-phosphorylating $\beta,\gamma$-bidentate chromium(III) complex of ATP ("CrATP"). In the wild type, CrATP binds with relatively low

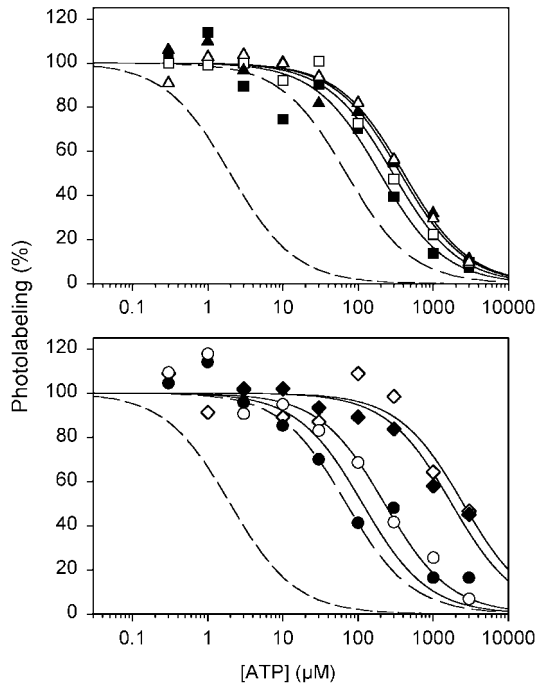


FIG. 5. **Binding of ATP determined by inhibition of TNP-8$N_3$-ATP photolabeling in the presence (*closed symbols*) or absence (*open symbols*) of $Mg^{2+}$.** Examples of data for Thr$^{441}$ → Ala (*squares*), Glu$^{442}$ → Ala (*triangles*), Arg$^{560}$ → Leu (*diamonds*), and Leu$^{562}$ → Phe (*circles*) are shown together with the best fits to the data for the expressed wild type obtained in the presence and absence of $Mg^{2+}$ (*short dashed* and *long dashed lines*, respectively) (5, 33). Photolabeling was performed in 25 mM EPPS/TMAH (pH 8.5), 20% (v/v) glycerol at a [$\gamma$-$^{32}$P]TNP-8$N_3$-ATP concentration of 3× $K_{0.5}$ and the indicated concentrations of ATP with either 1 mM $MgCl_2$ and 0.5 mM EGTA (presence of $Mg^{2+}$) or 2 mM EDTA (absence of $Mg^{2+}$). The *lines* show the best fits to the data of the equations described under "Experimental Procedures." Table I lists $K_D$ values derived in this way.

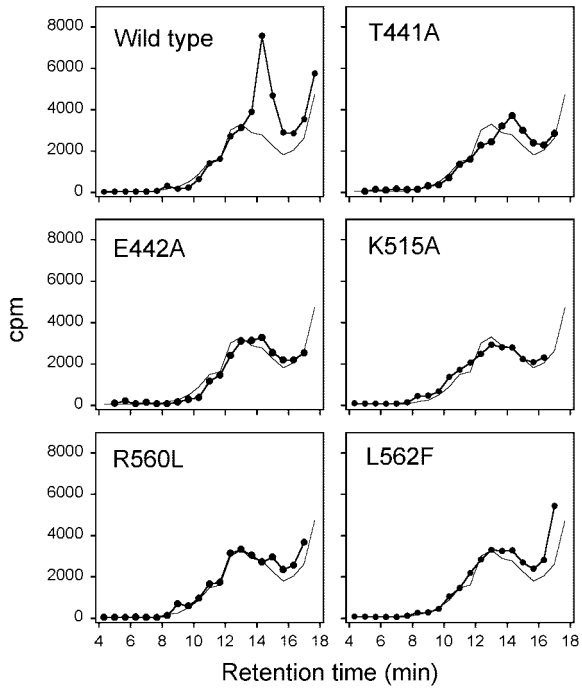


FIG. 6. **CrATP-dependent $Ca^{2+}$ occlusion.** Wild-type or mutant $Ca^{2+}$-ATPase expressed in COS-1 cell microsomes was incubated for 1 h at 37 °C in 50 mM TES/Tris (pH 7.0), 100 mM NaCl, 5 mM $MgCl_2$, 40 $\mu$M $^{45}CaCl_2$, and 1 mM CrATP. At the end of the incubation period, the membranes were solubilized by addition of 5 mg/ml of the non-ionic detergent $C_{12}E_8$. Following centrifugation, the supernatant was subjected to size-exclusion high pressure liquid chromatography as described previously (5). The elution buffer contained 50 mM TES/Tris (pH 7.0), 100 mM NaCl, 10 mM $MgCl_2$, 1.5 mM $CaCl_2$, 1 mM EGTA, and 2 mg/ml $C_{12}E_8$. The *solid circles* show the radioactivity in collected fractions. The result of a control experiment with microsomes harvested from cells transfected with the expression vector without insert is indicated by the *thin line without data points*. The difference between the test and control curves at 14–15 min of retention time, corresponding to the elution of $Ca^{2+}$-ATPase, provides a measure of the occluded $^{45}Ca^{2+}$. The amount of mutant $Ca^{2+}$-ATPase protein applied to the column was roughly equivalent to the amount of wild type (±30%, due to variation of the expression level, as determined by enzyme-linked immunosorbent assay).

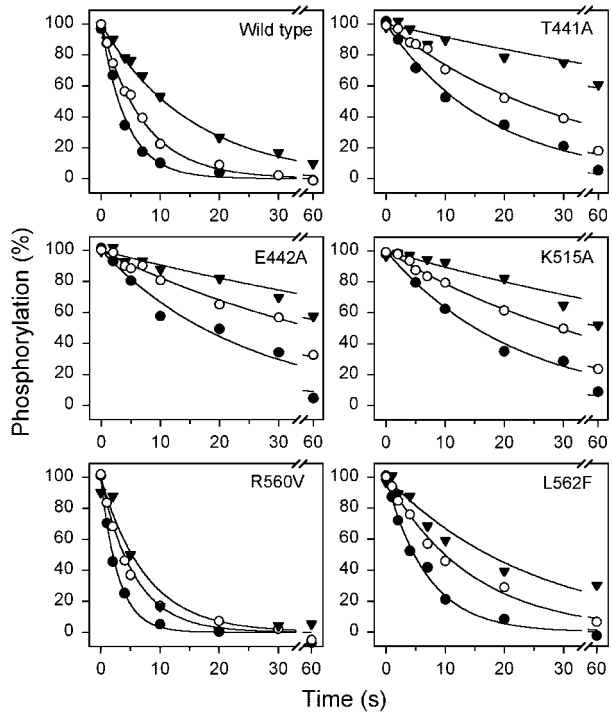


FIG. 7. **Dephosphorylation at 0 °C of phosphoenzyme formed from ATP.** Phosphorylation was performed for 15 s at 0 °C in a medium containing 40 mM MOPS/Tris (pH 7.0), 80 mM KCl, 5 mM $MgCl_2$, 1 mM EGTA, 0.955 mM $CaCl_2$ (giving a free $Ca^{2+}$ concentration during phosphorylation of 10 $\mu$M), 10 $\mu$M calcium ionophore A23187, and 5 $\mu$M [$\gamma$-$^{32}$P]ATP (50 $\mu$M in case of $Arg^{560} \rightarrow$ Val, because of its low affinity, *cf.* Fig. 2*A*). To measure dephosphorylation, the phosphoenzyme was chased by addition of 10 mM EGTA (*solid triangles*), 10 mM EGTA with 1 mM non-radioactive MgATP (*open circles*), or 10 mM EGTA with 5 mM non-radioactive MgATP (*solid circles*), and acid quenching was performed at the indicated time intervals. The *lines* show the best fits of a monoexponential decay function; the rate constants are listed in Table II.

affinity, forming a very stable complex with the enzyme, in which $Ca^{2+}$ is "occluded" at the transmembranous high affinity $Ca^{2+}$ sites (30, 35). The high stability of the $Ca^{2+}$-occluded CrATP-enzyme complex upon removal of free CrATP from the medium (35) makes it feasible to quantify the complex by size-exclusion chromatography of detergent-solubilized microsomal protein following incubation with CrATP in the presence of radioactive $^{45}Ca^{2+}$, and we have previously demonstrated a correlation between deficient CrATP-induced $^{45}Ca^{2+}$ occlusion and defective ATP binding in mutants of the $Ca^{2+}$-ATPase (5, 33). Because the $Ca^{2+}$ titration of ATPase activity described above indicated that all the mutant enzymes bind $Ca^{2+}$ with an affinity similar or close to that of wild type, the $Ca^{2+}$ sites are saturated at the $^{45}Ca^{2+}$ concentration of 40 $\mu$M used here, and the amount of $^{45}Ca^{2+}$ occluded should, therefore, reflect the ability to bind CrATP. Fig. 6 shows $^{45}Ca^{2+}$ elution profiles obtained for wild type and selected mutants, as well as for control microsomes harvested from cells transfected with the expression vector without insert. For wild type, a distinct peak is seen at 14–15 min of retention time, corresponding to the elution of $Ca^{2+}$-ATPase, whereas the control only shows a rather broad peak extending between 10 and 16 min of retention time. The difference between the test and control curves at 14–15 min of retention time provides a measure of $^{45}Ca^{2+}$ bound in the occluded state in the $Ca^{2+}$-ATPase. For mutant $Thr^{441} \rightarrow$ Ala, a minor peak of radioactivity was evident at the position corresponding to $Ca^{2+}$-ATPase, indicating partial, but extremely reduced, formation of the $Ca^{2+}$-occluded CrATP-enzyme complex in the present incubation conditions. No such peak was obtained in experiments performed with mutants $Glu^{442} \rightarrow$ Ala, $Lys^{515} \rightarrow$ Ala, $Arg^{560} \rightarrow$ Leu, and $Leu^{562} \rightarrow$ Phe (Fig. 6), or with $Arg^{560} \rightarrow$ Val and $Arg^{560} \rightarrow$ Glu (data not shown). For the $Cys^{561}$ mutants, the $^{45}Ca^{2+}$ peak corresponding to $Ca^{2+}$-ATPase was similar to that seen for wild type (data not shown). Thus, the effects of the mutations on formation of the $Ca^{2+}$-occluded CrATP-enzyme complex are in accordance with the effects on MgATP binding described above, and $Lys^{515} \rightarrow$ Ala is clearly included among the mutants showing defective nucleotide binding.

*The $E_1PCa_2$ to $E_2P$ Conformational Transition*—To examine the effects of the mutations on the $E_1PCa_2 \rightarrow E_2P$ transition, we determined the rate of decay of phosphoenzyme under conditions (0 °C, presence of $K^+$, and neutral pH) where the $E_1PCa_2 \rightarrow E_2P$ transition is rather slow and, thus, rate-limiting for the dephosphorylation, whereas the subsequent hydrolysis of $E_2P$ (Scheme 1) is relatively rapid. The phosphorylation by [$\gamma$-$^{32}$P]MgATP was terminated by addition of an excess of EGTA (to remove $Ca^{2+}$). As seen in Fig. 7 and Table II (column marked "EGTA," *i.e.* no addition of non-labeled MgATP), the rate of phosphoenzyme decay was reduced as much as 6–8-fold relative to wild type, for mutants $Thr^{441} \rightarrow$ Ala, $Glu^{442} \rightarrow$ Ala, and $Lys^{515} \rightarrow$ Ala. $Leu^{562} \rightarrow$ Phe deviated much less from wild type. Among the $Arg^{560}$ mutants, only $Arg^{560} \rightarrow$ Val could be examined, because of the very low phosphorylation levels ob-

TABLE II

*Dephosphorylation of phosphoenzyme formed from [$\gamma$-$^{32}$P]ATP or $^{32}P_i$*

Formation of $E_1PCa_2$ from [$\gamma$-$^{32}$P]ATP at 0 °C or of $E_2P$ from $^{32}P_i$ at 25 °C, and subsequent chase of the phosphoenzyme with dephosphorylation buffer containing excess EGTA (to terminate phosphorylation from [$\gamma$-$^{32}$P]ATP by removal of $Ca^{2+}$) or excess EDTA (to terminate phosphorylation from $^{32}P_i$ by removal of $Mg^{2+}$) and varying amounts of non-radioactive MgATP or ATP as indicated, was carried out as described in the legends to Figs. 7 and 9. A monoexponential decay function was fitted to the data, and the rate constant ($k_{dephos}$) is shown. ADP sensitivity was tested on phosphoenzyme formed from [$\gamma$-$^{32}$P]ATP by addition of 1 mM ADP with 10 mM EGTA (final concentrations), and the fraction of the phosphoenzyme remaining after 5 s ("*E*P") is shown.

| | $E_1PCa_2 \rightarrow E_2$ ($k_{dephos}$) | | | $E_1PCa_2 \rightarrow E_1$, 1 mM ADP, *EP* remaining after 5 s | $E_2P \rightarrow E_2$ ($k_{dephos}$) | |
|---|---|---|---|---|---|---|
| | EGTA | + 1 mM MgATP | + 5 mM MgATP | | EDTA | + 1 mM ATP |
| | | *min*$^{-1}$ | | % | *min*$^{-1}$ | |
| Wild type | 3.9 | 8.3 | 13.8 | 2.9 | 1.9 | 3.7 |
| $Thr^{441} \rightarrow Ala$ | 0.5 | 1.8 | 3.4 | 7.6 | 2.6 | 5.6 |
| $Glu^{442} \rightarrow Ala$ | 0.6 | 1.2 | 2.4 | 3.5 | 10.2 | 17.4 |
| $Lys^{515} \rightarrow Ala$ | 0.7 | 1.4 | 2.7 | 4.5 | 6.8 | 10.3 |
| $Arg^{560} \rightarrow Leu$[a] | | | | | 1.5 | 3.9 |
| $Arg^{560} \rightarrow Val$ | 7.9 | 10.6 | 20.4 | 24.1 | 1.7 | 5.0 |
| $Arg^{560} \rightarrow Glu$[a] | | | | | 9.8 | 17.4 |
| $Leu^{562} \rightarrow Phe$ | 2.4 | 4.2 | 8.7 | 4.3 | 2.3 | 4.9 |
| $Phe^{487} \rightarrow Ser$[a] | | | | | 2.6 | 4.4 |
| $Phe^{487} \rightarrow Leu$ | 2.6 | 3.1 | 5.1 | 2.9 | 3.0 | 6.9 |
| $Arg^{489} \rightarrow Leu$ | 4.7 | 7.4 | 11.7 | 8.7 | 3.1 | 5.7 |
| $Lys^{492} \rightarrow Leu$ | 0.7 | 1.4 | 1.9 | 3.3 | 4.7 | 8.8 |

[a] Only studies of $E_2P \rightarrow E_2$ of $P_i$-phosphorylated enzyme were carried out with these mutants due to the low level of phosphoenzyme formed from ATP.

tained with the other two $Arg^{560}$ mutants at 0 °C. It appears from Fig. 7 and Table II that $Arg^{560} \rightarrow Val$ showed a unique 2-fold enhancement of the rate of phosphoenzyme decay, relative to wild type.

To test the low affinity modulatory effect of the nucleotide on the $E_1PCa_2 \rightarrow E_2P$ transition (*cf.* Scheme 1, *boxed ATP*), the dephosphorylation was also examined at 1 and 5 mM non-labeled MgATP added with EGTA. It can be seen in Fig. 7 and Table II that the nucleotide induced a significant enhancement of the dephosphorylation rate in the wild type as well as the mutants. Both in wild type and in $Thr^{441} \rightarrow Ala$, $Glu^{442} \rightarrow Ala$, $Lys^{515} \rightarrow Ala$, $Arg^{560} \rightarrow Val$, and $Leu^{562} \rightarrow Phe$ the rate constant observed at 5 mM MgATP was roughly 2-fold higher than that observed at 1 mM MgATP, which is surprisingly consistent with the increase of ATPase activity in this concentration range (Fig. 3), taking into account the different temperatures under which these experiments were carried out.

Table II also shows the results of similar measurements performed with mutants $Phe^{487} \rightarrow Leu$, $Arg^{489} \rightarrow Leu$, and $Lys^{492} \rightarrow Leu$, whose MgATP and ATP affinities at the substrate site were reported in the previous paper (5) and in Table I of the present paper, respectively. $Lys^{492} \rightarrow Leu$ showed a conspicuous 6-fold slowing of the phosphoenzyme decay observed upon EGTA addition, whereas only small differences from wild type were seen for $Phe^{487} \rightarrow Leu$ and $Arg^{489} \rightarrow Leu$. For all 3 mutants, there was a substantial modulatory effect of millimolar MgATP, although slightly less pronounced than for the wild type and the above-described mutants (1.4–1.6-fold enhancement from 1 to 5 mM MgATP).

*ADP Sensitivity of the Phosphoenzyme*—The two phosphoenzyme intermediates $E_1PCa_2$ and $E_2P$ can normally be distinguished by their different sensitivity to ADP. $E_1PCa_2$ is ADP-sensitive, *i.e.* able to donate the phosphoryl group back to ADP, forming ATP, whereas $E_2P$ is insensitive to ADP and dephosphorylates only by hydrolysis. To test the ADP sensitivity, 1 mM ADP was added following phosphorylation under the same conditions as described for Fig. 7. This resulted in almost complete dephosphorylation of wild type within 5 s, demonstrating accumulation of the $E_1PCa_2$ form of the phosphoenzyme, and similar effects of ADP were seen for all the mutants studied except $Arg^{560} \rightarrow Val$, for which as much as 24% phosphoenzyme remained after the 5-s incubation with ADP (Table II), indicating a significantly reduced sensitivity to ADP. This could be the result of accumulation of $E_2P$, as a consequence of the enhancement of the $E_1PCa_2 \rightarrow E_2P$ transition reported above. Alternatively, the reduced ADP sensitivity reflects a lowered affinity of the $E_1PCa_2$ form for ADP. This would be in keeping with the very pronounced decrease in affinity for MgADP and ADP shown above for $Arg^{560} \rightarrow Leu$ (Table I).

*Properties of the $E_2P$ Phosphoenzyme*—The $E_2P$ phosphoenzyme can be formed by "backward" phosphorylation with inorganic phosphate of the $E_2$ state in the absence of $Ca^{2+}$ and presence of $Mg^{2+}$ (*cf.* Scheme 1). Fig. 8 shows the phosphorylation at varying concentrations of $^{32}P_i$ under conditions optimal for stabilization of the $E_2P$ phosphoenzyme (acidic pH, presence of the organic solvent dimethyl sulfoxide, and absence of alkali metal ions). The concentration of $P_i$ giving half-maximum phosphorylation is close to 10 $\mu$M for wild type. Significantly reduced apparent affinity (increased $K_{0.5}$) for $P_i$ was seen for $Glu^{442} \rightarrow Ala$ and $Lys^{515} \rightarrow Ala$ (5- and 2.5-fold, respectively), whereas $Arg^{560} \rightarrow Leu$ and $Arg^{560} \rightarrow Val$ showed 2-fold increased apparent affinity for $P_i$. Minor shifts were also seen for mutants $Thr^{441} \rightarrow Ala$ and $Cys^{561} \rightarrow Ala$ ($K_{0.5}$ 1.5-fold increased and 1.5-fold decreased, respectively), whereas mutants $Arg^{560} \rightarrow Glu$ and $Leu^{562} \rightarrow Phe$ (Fig. 8), as well as $Cys^{561} \rightarrow Trp$ (not shown), were indistinguishable from wild type. It is important to stress here that because the $K_{0.5}$ is a function of several kinetic constants, it should not necessarily correlate with the true dissociation constant, $K_D$, describing the non-covalent enzyme-$P_i$ complex ($E_2 \cdot P_i$ in Scheme 1). As discussed previously (34), the respective rate constants, $k_2$ and $k_{-2}$, for formation and hydrolysis of the covalent bond in $E_2P$ may be important as well. To study $k_{-2}$, the wild type and selected mutants were phosphorylated under optimal conditions for formation of the $E_2P$ phosphoenzyme, followed by dilution at 25 °C into a medium of the same composition except for the absence of radioactively labeled $P_i$, a reduction of the dimethyl sulfoxide concentration from 30 to 15%, and the presence of excess EDTA to remove free $Mg^{2+}$ and thus terminate phosphorylation (Fig. 9 and Table II). It should be noted that because of the acidic pH, absence of $K^+$, and presence of 15% dimethyl sulfoxide, the rate of dephosphorylation of $E_2P$ is

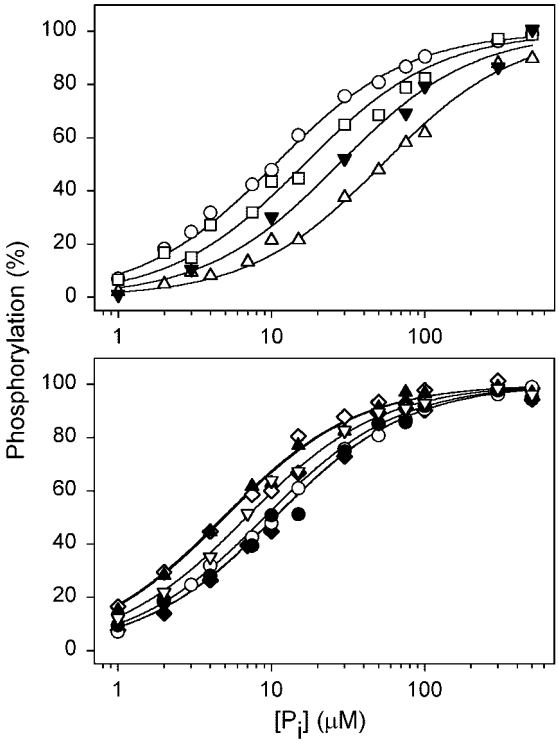


FIG. 8. **Phosphorylation from $P_i$.** Wild type and mutants were phosphorylated at 25 °C for 10 min in a medium containing 100 mM MES/Tris (pH 6.0), 2 mM EGTA, 30% (v/v) dimethyl sulfoxide, 10 mM $MgCl_2$, and varying concentrations of $^{32}P_i$ as indicated. The *lines* show the best fits of the Hill equation with the Hill coefficient set to 1, giving the $K_{0.5}$ values (in μM ± S.E.) indicated in *parentheses*: *open circles*, wild type (10.5 ± 0.6); *open squares*, $Thr^{441} \rightarrow Ala$ (16.4 ± 1.5); *open triangles*, $Glu^{442} \rightarrow Ala$ (52.8 ± 8.2); *reversed solid triangles*, $Lys^{515} \rightarrow Ala$ (27.5 ± 5.2); *open diamonds*, $Arg^{560} \rightarrow Leu$ (4.8 ± 0.4); *solid triangles*, $Arg^{560} \rightarrow Val$ (5.0 ± 0.4); *solid diamonds*, $Arg^{560} \rightarrow Glu$ (9.0 ± 1.0); *reversed open triangles*, $Cys^{561} \rightarrow Ala$ (6.9 ± 0.4); and *solid circles*, $Leu^{562} \rightarrow Phe$ (10.6 ± 0.9). The 100% value corresponds to the phosphorylation level reached at infinite $P_i$ concentration as deduced from the fit.

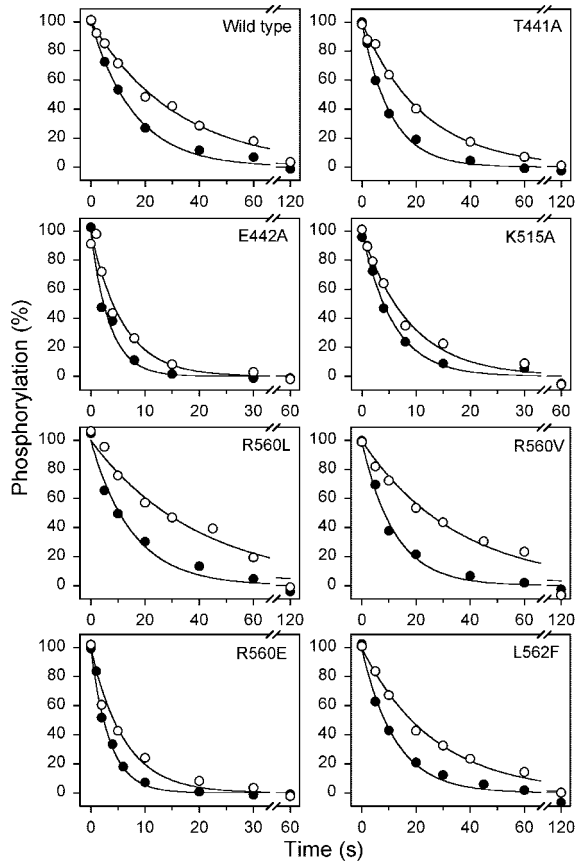


FIG. 9. **Dephosphorylation of phosphoenzyme formed from $P_i$.** Wild type and mutants were phosphorylated at 25 °C for 10 min in a medium containing 100 mM MES/Tris (pH 6.0), 2 mM EGTA, 30% (v/v) dimethyl sulfoxide, 10 mM $MgCl_2$, and 0.5 mM $^{32}P_i$. Dephosphorylation was studied at 25 °C by a 19-fold dilution into a medium containing EDTA (to remove free $Mg^{2+}$) corresponding to a final concentration of 10 mM, 100 mM MES/Tris (pH 6.0), 2 mM EGTA, 15% (v/v) dimethyl sulfoxide, 0.5 mM non-radioactive $P_i$, without (*open circles*) or with (*solid circles*) 1 mM ATP, followed by acid quenching at serial time intervals. The *lines* show the best fits of a monoexponential decay function; the rate constants are listed in Table II.

much slower than under physiological conditions. For mutants $Glu^{442} \rightarrow Ala$ and $Lys^{515} \rightarrow Ala$, the reduced apparent affinities for $P_i$ (Fig. 8) were well accounted for by significantly increased rates of $E_2P$ hydrolysis (5- and 3.5-fold, respectively). A similar increase was noted for $Lys^{492} \rightarrow Leu$ (Table II). For mutant $Thr^{441} \rightarrow Ala$, a slightly (1.4-fold) increased rate of $E_2P$ hydrolysis (Fig. 9) explains the 1.5-fold increased $K_{0.5}$ (Fig. 8). $Leu^{562} \rightarrow Phe$, $Phe^{487} \rightarrow Ser$, $Phe^{487} \rightarrow Leu$, and $Arg^{489} \rightarrow Leu$ also showed slight increases of the rate of $E_2P$ hydrolysis, and the $Cys^{561}$ mutants (data not shown) were indistinguishable from wild type. Interestingly, mutant $Arg^{560} \rightarrow Glu$ showed a conspicuous 5-fold increase of the rate of $E_2P$ hydrolysis (Fig. 9), despite its wild type-like apparent affinity for $P_i$ (Fig. 8). In analogy with this discrepancy, mutants $Arg^{560} \rightarrow Leu$ and $Arg^{560} \rightarrow Val$ showed wild type-like rates of $E_2P$ hydrolysis (Fig. 9), but 2-fold increased apparent affinities for $P_i$ (Fig. 8). Thus, for the $Arg^{560}$ mutants, an increase of the true affinity for $P_i$ ($K_D$) or an increased rate constant for formation of the covalent bond in $E_2P$ ($k_2$) must contribute to the change (and lack thereof) in the apparent affinity for $P_i$.

Fig. 9 and Table II furthermore show that inclusion of 1 mM ATP enhanced the dephosphorylation of $E_2P$ close to 2-fold in the wild type and all the mutants studied, thus indicating that the modulatory effect of ATP on this partial reaction step (*cf. boxed* ATP in Scheme 1) is as unaffected by the mutations as the low affinity modulatory effect on the $E_1PCa_2 \rightarrow E_2P$ transition described above. Because the modulation of $E_2P \rightarrow E_2$ has been ascribed to metal-free ATP rather than the MgATP complex (14), it is important to note here that when ATP was included in the assay for dephosphorylation of $E_2P$, the ATP was present in the metal-free form as a consequence of the co-addition of excess EDTA, unlike the assay for the $E_1PCa_2 \rightarrow E_2P$ transition described above, where the major fraction of the ATP was present as MgATP.

*Reaction of $Lys^{515}$ with FITC*—FITC is a potent inhibitor of $Ca^{2+}$-ATPase activity (2) and acts by specific covalent attachment to $Lys^{515}$ (3), blocking high affinity ATP binding (2). The specificity of the reaction is mainly due to a high affinity of FITC for the nucleotide site rather than an unusual high reactivity of $Lys^{515}$ (36). Because the side chains of $Lys^{515}$ and $Glu^{442}$ are in close proximity, facing each other in the crystal structure of the $Ca^{2+}$-ATPase (1), we considered that functionally important interaction between them might occur in the native enzyme and that this might be revealed by testing the effect of the $Glu^{442} \rightarrow Ala$ mutation on the reactivity of $Lys^{515}$ toward FITC. The kinetics of the reaction of FITC with wild type and mutant $Glu^{442} \rightarrow Ala$ is shown in Fig. 10*A*. The reaction was monitored by taking advantage of the inhibition of [γ-$^{32}$P]TNP-8$N_3$-ATP photolabeling by FITC binding. At 2 μM FITC, the half-time for the reaction of wild type with FITC was ~2 min. In contrast, the reaction of mutant $Glu^{442} \rightarrow Ala$ was too fast to measure, being completed in less than 15 s. At 0.2 μM

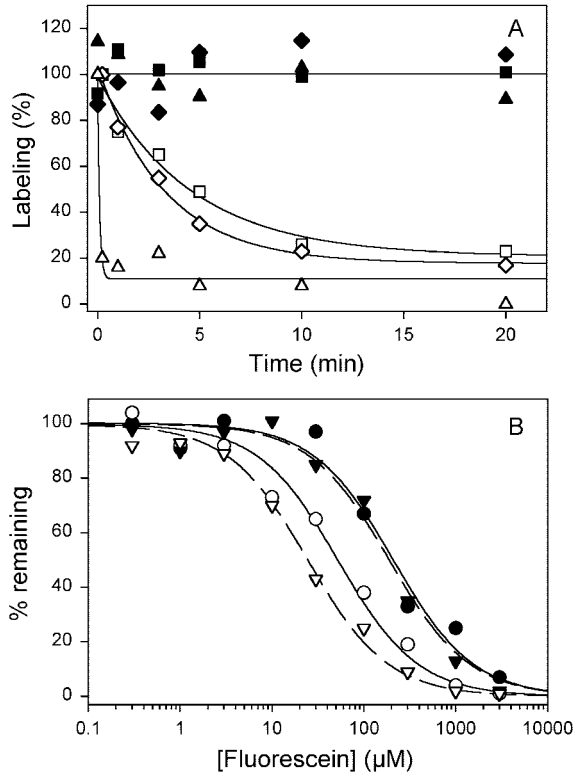


FIG. 10. **Kinetics of FITC reaction (*A*) and concentration dependence of fluorescein binding (*B*) to wild type and mutant $Glu^{442} \rightarrow Ala$ as determined by inhibition of TNP-$8N_3$-ATP photolabeling.** *A*, the FITC reaction (*open symbols*) with wild type (*diamonds*) or mutant $Glu^{442} \rightarrow Ala$ (*triangles* and *squares*) was performed in 25 mM ammonium bicarbonate, pH 7.8, 1 mM $MgCl_2$, 0.5 mM EDTA, 0.3 M sucrose, 0.2 (*squares*) or 2 (*diamonds* and *triangles*) $\mu$M FITC, and 10–15 pmol/ml $Ca^{2+}$-ATPase. Controls (*solid symbols*) did not contain FITC. The reaction was terminated at the time intervals shown, by diluting aliquots 4.2-fold into ice-cold irradiation medium to yield final concentrations of 25 mM EPPS/TMAH, pH 8.5, 1.24 mM $MgCl_2$, 0.5 mM EGTA, 0.12 mM EDTA, 20% (v/v) glycerol, 2 $\mu$M [$\gamma$-$^{32}$P]TNP-$8N_3$-ATP, and 2.4–3.6 pmol/ml $Ca^{2+}$-ATPase. The suspensions were irradiated for 1 min, the protein solubilized and subjected to SDS-PAGE, and the relevant bands quantified. *B*, inhibition of [$\gamma$-$^{32}$P]TNP-$8N_3$-ATP photolabeling by fluorescein in wild type (*circles*) and mutant $Glu^{442} \rightarrow Ala$ (*triangles*) as described for MgATP in the legend to Fig. 5. The concentrations of [$\gamma$-$^{32}$P]TNP-$8N_3$-ATP were close to the $K_{0.5}$ (0.79 $\mu$M for wild type, 0.46 $\mu$M for mutant $Glu^{442} \rightarrow Ala$, cf. Table I) (*solid symbols*) or to 0.25× $K_{0.5}$ (*open symbols*). The *lines* show the best fits using the Hill equation. Average true $K_D$ values for fluorescein binding of 47 $\mu$M and 34 $\mu$M for wild type and $Glu^{442} \rightarrow Ala$, respectively, were derived from the $K_{0.5}$ values at the two concentrations of photolabel using the competitive binding equation provided in Ref. 5.

FITC, the kinetics of the mutant resembled that of the wild type at 2 $\mu$M (Fig. 10*A*). The rapid reaction with FITC seen for the mutant could either be due to an increased binding affinity of the mutant enzyme for FITC or a true increase in the rate constant for the covalent reaction. Note that the concentration of FITC during the reaction was much lower than the $K_D$ for FITC binding (70 $\mu$M according to Ref. 36, also see below for the value of fluorescein), meaning that an increase in affinity, and proportion of bound FITC, could have a significant effect on the kinetics. To distinguish between these two possibilities, we determined whether the mutation altered the affinity for fluorescein, which is similar to FITC except it lacks the reactive isothiocyanate group. The isothiocyanate group, however, is unlikely to contribute significantly to the binding energy as it is involved in the chemical reaction. As for FITC, the binding of fluorescein was measured through the competitive inhibition of photolabeling, and the results are shown in Fig 10*B*. At two different concentrations of [$\gamma$-$^{32}$P]TNP-$8N_3$-ATP, the $K_D$ values

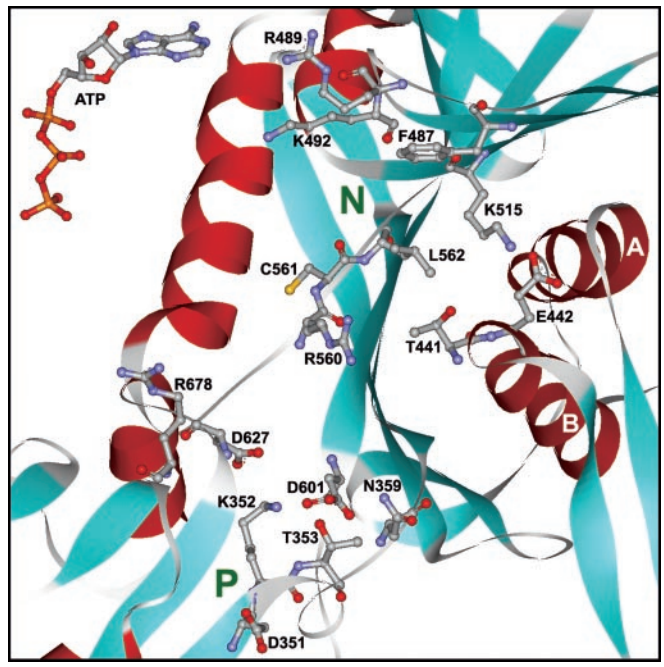


FIG. 11. **Positions of key residues discussed, in the $E_1Ca_2$ crystal structure of the $Ca^{2+}$-ATPase.** The view is down toward the membrane from the cytoplasmic side. Carbon atoms are shown in *gray*, nitrogen in *blue*, oxygen in *red*, sulfur in *yellow*, and phosphorus in *orange*. Schematic representations of $\alpha$-helices and $\beta$-strands are shown in *red* and *cyan*, respectively. Residues discussed in the text are labeled. An ATP molecule in a conformation that could fit into the nucleotide-binding site is depicted in the *top-left corner*. *N*, nucleotide-binding domain; *P*, phosphorylation domain. Helices labeled *A* and *B* indicate the two central *N*-domain helices with sequences $^{407}$FDGLVELATICALCN$^{421}$ and $^{441}$TETALTTLVEKMN$^{453}$, respectively. Prepared by use of WebLab Viewer Pro (Molecular Simulations Ltd., Cambridge, England), using the atomic coordinates obtained from the Protein Data Bank under accession code 1EUL (1).

for fluorescein binding to wild type and mutant $Glu^{442} \rightarrow Ala$ were similar, the average values being 47 and 34 $\mu$M, respectively (see figure legend). Hence, the effect of the mutation on the reaction with FITC must be largely due to an increase in the rate constant corresponding to the covalent reaction.

## DISCUSSION

In this study, we show for the first time, using a direct binding assay, that amino acids $Thr^{441}$ and $Glu^{442}$ of the $^{441}$TETAL helix and $Lys^{515}$, $Arg^{560}$, and $Leu^{562}$ of two central $\beta$-strands, all in domain *N*, are crucial to MgATP binding at the substrate site. Subsequent catalytic steps were also affected by the mutations. $Arg^{560}$ seems to play a critical role in optimizing the rate of phosphoryl transfer from the substrate to $Asp^{351}$, and the $Arg^{560} \rightarrow Val$ mutation furthermore enhanced the rate of the $Ca^{2+}$-translocating $E_1PCa_2 \rightarrow E_2P$ conformational transition, whereas this transition was slowed substantially by alteration to $Thr^{441}$, $Glu^{442}$, $Lys^{515}$, or $Lys^{492}$. Moreover, some of the mutations influenced the hydrolysis of $E_2P$. On the other hand, none of the residues examined seems very important for the binding of modulatory nucleotide to the phosphoenzyme.

The crystal structure of the $Ca^{2+}$-ATPase has revealed that domain *N* is composed of a seven-stranded anti-parallel $\beta$-sheet arranged as a half-barrel wrapped around two central helices, with sequences $^{407}$FDGLVELATICALCN$^{421}$ and $^{441}$TETALTTLVEKMN$^{453}$ (helices labeled *A* and *B*, respectively, in Fig. 11). The $\beta$-sheet is made up of two sections; one is linked to two hinge segments, incorporating $Asp^{601}$ and $Asn^{359}$ leading to and from domain *P*. The inner edge/strand of this portion of the sheet is made up of segment $^{560}$RCLALA. The second part of the sheet, incorporating segments $^{487}$FSRDRK and $^{515}$KGAPE,

protrudes from the domain. Our results here, in conjunction with a previous study (5), support the hypothesis that the MgATP high affinity binding site is composed of elements of $^{441}$TETAL, $^{487}$FSRDRK, $^{515}$KGAPE, and $^{560}$RCLALA. The adenine five-membered ring could fit in the gap between the side chains of Phe$^{487}$ and Leu$^{562}$ (*cf.* Fig. 11), such that, depending on the orientation, the 8- or 2-position of the base faces Lys$^{492}$, in the former case accounting for the photolabeling of this residue with TNP-8$N_3$-ATP. Glu$^{442}$ and Lys$^{515}$ are buried deep in the binding pocket and may interact with the six-membered ring of the adenine moiety. The fact that even the bulky tryptophan replacement of Cys$^{561}$ was without much influence on nucleotide binding supports these ideas, as Cys$^{561}$ points away from the putative binding pocket formed by the critical residues. The bound nucleotide would link the structural elements of the nucleotide-binding site in a manner that could stabilize a closer interaction, as part of the nucleotide-induced conformational change previously detected (37–40).

Thr$^{441}$, Glu$^{442}$, and Leu$^{562}$ cluster together in the binding pocket, and the consequences of mutations here for nucleotide binding were rather similar (Table I). MgATP binding was strongly disturbed (70–180-fold increase of $K_D$), whereas the affinity for uncomplexed ATP was much less affected (only 2–5-fold increase of $K_D$). The resulting affinities for ATP and MgATP were very similar, thus demonstrating that these mutants are rather insensitive to $Mg^{2+}$. For Thr$^{441}$ → Ala, the $K_D$ values for ADP and MgADP also differed significantly less (~2-fold) as compared with wild type (~7-fold). Furthermore, the ability to respond to $Mg^{2+}$ with a reduced affinity for the TNP-nucleotide was lost in Thr$^{441}$ → Ala. One possible cause of these effects is interference with the interaction between the protein and the $Mg^{2+}$ ion complexed by the nucleotide, implying that at least Thr$^{441}$ could be a $Mg^{2+}$-ligating residue in the initial encounter of the nucleotide with the binding site. This possibility is consistent with recent evidence from $Fe^{2+}$-catalyzed oxidation, suggesting that the metal ion of FeATP interacts close to Thr$^{441}$ in the $Ca^{2+}$-ATPase and in the $Na^+$,$K^+$-ATPase close to the residue equivalent to Glu$^{439}$ (41, 42). Interestingly, mutations of Thr$^{353}$ in domain *P* are also more detrimental to MgATP binding as compared with ATP binding, and in some non-ATPase members of the family of aspartyl phosphate-utilizing phosphohydrolases and phosphotransferases the residue equivalent to Thr$^{353}$ of the $Ca^{2+}$-ATPase has been shown to be involved in $Mg^{2+}$ ligation (see Ref. 34 and references therein). On the basis of the crystal structure (Fig. 11), it is not unrealistic to think that upon nucleotide binding the Thr$^{441}$/Glu$^{442}$/Leu$^{562}$ cluster could come close to Thr$^{353}$ or that the $Mg^{2+}$ ion initially complexed with ATP could move from a site near Thr$^{441}$ to a site involving Thr$^{353}$. As an alternative, the preferential loss of affinity for the $Mg^{2+}$-complexed forms of ATP and ADP seen for Thr$^{441}$ → Ala, Glu$^{442}$ → Ala, and Leu$^{562}$ → Phe could be explained without having to assume a direct interaction with $Mg^{2+}$, if these residues interact only with the nucleotide *per se*, and the $Mg^{2+}$ ion complexed by the nucleotide assists the docking of the phosphoryl part in domain *P* in such a way that it changes the position of the rest of the nucleotide and, thus, its interaction with the mutated residues. Thereby, the contributions of these residues to the binding energy would depend on $Mg^{2+}$. In other words, the site binding ATP differs somewhat from the binding site for the MgATP complex.

In contrast to the above-mentioned mutants, pronounced effects on nucleotide binding in the absence of $Mg^{2+}$ were seen for mutants Arg$^{489}$ → Leu and Lys$^{492}$ → Tyr (Table I). In this connection, it is interesting to note that Lys$^{492}$ is cross-linked to Arg$^{678}$ in domain *P* by glutaraldehyde in what is likely to be a zero distance linkage (43), and the clustering of the three positive charges of Arg$^{489}$, Lys$^{492}$, and Arg$^{678}$ could make interaction with phosphates energetically very favorable. This is also where decavanadate binds (1, 44). Thus, at least in the absence of $Mg^{2+}$, parts of the phosphate chain could interact with these basic residues.

Mutation of Arg$^{560}$ to leucine was shown to be detrimental both to ATP and ADP binding, in the absence as well as in the presence of $Mg^{2+}$ (Table I). The very large effects of the Arg$^{560}$ → Leu mutation on ADP and MgADP binding support a role for the positive charge of the guanidino group of Arg$^{560}$ in interaction with the β-phosphoryl, the α-phosphoryl, ribose, or adenine. Neither of these possibilities can be excluded on the basis of the two published crystal structures of the enzyme. Modeling of MgATP into the structure of the $E_2$ form with bound thapsigargin, bringing the $Mg^{2+}$ ion complexed between the β- and γ-phosphates of ATP close to the side-chain oxygens of Thr$^{441}$ and Glu$^{442}$, suggested contribution of Arg$^{560}$ to ligation of adenine (41). In $E_1Ca_2$ crystals soaked with TNP-AMP (1), Arg$^{560}$ is pointing toward the TNP moiety, suggesting that Arg$^{560}$ could be interacting with the 2′- and/or 3′-hydroxyl of the ribose in ATP. Our data on TNP-nucleotide binding to Arg$^{560}$ mutants in the presence of $Mg^{2+}$ are compatible with the interaction between the TNP moiety and Arg$^{560}$ observed in the crystals, in the presence of $Mg^{2+}$. Rather surprisingly, in Arg$^{560}$ → Leu, the binding of TNP-8$N_3$-ATP was hardly disturbed in the absence of $Mg^{2+}$. Hence, Arg$^{560}$ is not essential to the binding of the TNP moiety in this condition, lending further support to the hypothesis that $Mg^{2+}$ changes the position of bound nucleotide.

The role of Arg$^{560}$ does not seem to be confined to merely binding the nucleotide. The Arg$^{560}$ mutants showed substantially reduced steady-state levels of phosphoenzyme (Figs. 1 and 2*A*) and of acetyl phosphate-supported $Ca^{2+}$ transport (Fig. 4). It has been demonstrated for the wild type that in addition to the rate of the $E_1PCa_2$ → $E_2P$ transition (*cf.* Scheme 1), the rate of formation of $E_1PCa_2$ is limiting for the $Ca^{2+}$ transport rate attainable with acetyl phosphate as substrate (16). We were able to demonstrate that the $E_1PCa_2$ → $E_2P$ transition rate is, in fact, enhanced in Arg$^{560}$ → Val (Fig. 7). Thus, it seems likely that the rate of formation of $E_1PCa_2$ is reduced in this mutant. Furthermore, mutation Arg$^{560}$ → Val was less detrimental to MgATP binding (40-fold decrease of affinity) than the mutations of Thr$^{441}$ and Glu$^{442}$ (>120-fold decrease of affinity, Table I), and yet the $K_{0.5}$ for MgATP dependence of phosphorylation was much higher for Arg$^{560}$ → Val than for the latter mutants (Fig. 2*A*). The $K_{0.5}$ depends on the intrinsic (true) affinity for MgATP, determined in the binding assay, as well as the rate constant for transfer of the phosphoryl group from ATP to the enzyme. Therefore, the high $K_{0.5}$ observed for Arg$^{560}$ → Val may reflect a role of Arg$^{560}$ in the latter reaction. The low ATPase activity, even at saturating MgATP concentrations, and lack of activation by calcium ionophore, seen in all the Arg$^{560}$ mutants (Fig. 1), is also consistent with a slow, rate-limiting phosphorylation step, because activation by ionophore requires that the $E_1PCa_2$ → $E_2P$ transition, sensitive to inhibition by lumenal $Ca^{2+}$, is rate-limiting (26). It all points to mutations of Arg$^{560}$ as affecting not only nucleotide binding but also phosphoryl transfer. This could mean that in the transition state existing during phosphoryl transfer, Arg$^{560}$ has important interaction with the γ-phosphoryl group of ATP in addition to the β-phosphoryl, in line with a suggestion for the corresponding arginine of the $Na^+$,$K^+$-ATPase (45). There are, however, alternative possibilities. On the basis of the crystal structure of $E_1Ca_2$, one can predict that Arg$^{560}$ could come very close to Asp$^{627}$ when domain *N* ap-

proaches domain *P* for phosphorylation. Because $Asp^{627}$ points toward $Lys^{352}$ (*cf.* Fig. 11), a critical ATP binding and catalytic residue (33), the $Arg^{560}$–$Asp^{627}$ interaction may be necessary to allow $Lys^{352}$ to interact with the substrate. It is understandable in this scenario how mutation of the arginine could affect phosphorylation.

Unlike the $Arg^{560}$ mutants, $Leu^{562} \rightarrow$ Phe showed a normal rate of acetyl phosphate-supported $Ca^{2+}$ transport (Fig. 4), despite markedly reduced rates of ATP-driven $Ca^{2+}$ transport and ATPase activity, and lack of ionophore activation of the latter reaction (Fig. 1). This means that the role of $Leu^{562}$ to a large extent is nucleotide-specific. In $Leu^{562} \rightarrow$ Phe, the rate of phosphoryl transfer may very well be reduced relative to wild type with MgATP as substrate but not with acetyl phosphate as substrate. A reduced rate constant for phosphoryl transfer from MgATP in $Leu^{562} \rightarrow$ Phe would be consistent with the finding that the $K_{0.5}$ for MgATP dependence of phosphorylation was higher for $Leu^{562} \rightarrow$ Phe than for $Glu^{442} \rightarrow$ Ala (Fig. 2*A*), whereas the $K_D$ value for MgATP determined in the binding assay was highest for $Glu^{442} \rightarrow$ Ala (Table I).

$Lys^{515}$ lies deep in the binding cleft and is the residue that reacts with FITC (3). Mutation of $Lys^{515}$ to alanine prevented TNP-$8N_3$-ATP photolabeling of $Lys^{492}$, showing that the adenine positioning in relation to the latter residue was disturbed. CrATP binding was also eliminated in $Lys^{515} \rightarrow$ Ala (Fig. 6), indicating that the binding deficiency is not confined to the TNP-nucleotide. $Glu^{442}$ points toward $Lys^{515}$ in the crystal structure (Fig. 11), and we found that the reactivity of the amino group of $Lys^{515}$ was profoundly increased by mutation $Glu^{442} \rightarrow$ Ala, indicating that the amino group was changed into the more reactive uncharged form as a consequence of the elimination of the charge on residue 442. This suggests that in the native wild-type enzyme the two residues are ion-paired, forming a salt link, in accordance with the structure of the crystallized enzyme (1). Ion pairs are not favored over the neutral forms in a low dielectric medium, unless strengthened by additional hydrogen bonding (46). It is evident from the crystal structure that these two residues are both likely to hydrogen-bond to backbone amides and/or carbonyls at the end of the $^{407}$FDGLVELATICALCN$^{421}$ helix (Fig. 11). Strengthening the salt link may be important for the nucleotide-induced conformational change alluded to above, thus aiding the interaction of the secondary flange, where $Lys^{515}$ resides, with the $^{441}$TETAL helix. Thus the lysine and the glutamate may have dual roles, one in nucleotide ligation and the other as a clasp linking two key structural elements in the binding site.

For $Glu^{442} \rightarrow$ Ala and $Lys^{515} \rightarrow$ Ala, the reduced $k_{obs}$ values for phosphorylation seen in the presence of 5 $\mu$M MgATP (Fig. 2*B*) seem to be well explained by the poor nucleotide affinity, resulting in a low fraction of enzyme with bound nucleotide. In $Thr^{441} \rightarrow$ Ala, on the other hand, the rate constant for phosphoryl transfer from MgATP may be somewhat reduced, relative to $Glu^{442} \rightarrow$ Ala, because the $K_{0.5}$ for MgATP dependence of phosphorylation (Fig. 2*A*) and the $k_{obs}$ for phosphorylation (Fig. 2*B*) were more strongly affected in $Thr^{441} \rightarrow$ Ala than in $Glu^{442} \rightarrow$ Ala, whereas the opposite was the case for the $K_D$ for MgATP determined in the binding assay (Table I) and the ability to bind CrATP (Fig. 6).

As demonstrated by the data in Fig. 7 and Table II, $Thr^{441} \rightarrow$ Ala, $Glu^{442} \rightarrow$ Ala, $Lys^{492} \rightarrow$ Leu, and $Lys^{515} \rightarrow$ Ala showed a conspicuous 6–8-fold reduction of the rate of the $E_1PCa_2 \rightarrow E_2P$ conversion. This contrasts with the 2-fold enhancement seen for $Arg^{560} \rightarrow$ Val (for $Arg^{560} \rightarrow$ Glu and $Arg^{560} \rightarrow$ Leu, the $E_1PCa_2 \rightarrow E_2P$ transition could not be studied, because of the low phosphorylation level with nucleotide substrate). The strongly reduced rate of the $E_1PCa_2 \rightarrow E_2P$ conversion explains the decrease in acetyl phosphate-supported $Ca^{2+}$ transport observed for $Thr^{441} \rightarrow$ Ala, $Glu^{442} \rightarrow$ Ala, and $Lys^{515} \rightarrow$ Ala (Fig. 4), without necessarily having to assume a reduced rate of the phosphorylation step in these cases. Moreover, the reduced maximum rate of ATP hydrolysis seen with these mutants (Fig. 3) can be explained by the reduced rate of the $E_1PCa_2 \rightarrow E_2P$ conversion, and the enhancement seen upon addition of ionophore (Fig. 1) is consistent with a rate-limiting role of the $E_1PCa_2 \rightarrow E_2P$ conversion (26), in contrast to the lack of ionophore effect seen for the mutants with alteration to $Arg^{560}$ or $Leu^{562}$.

Previously, a number of point mutations, mainly located in the cytoplasmic domains *A* and *P* and in the segment connecting transmembrane segment M4 with domain *P*, have been shown to inhibit the $E_1PCa_2 \rightarrow E_2P$ transition (22, 25, 28, 34, 47–49). $Thr^{441} \rightarrow$ Ala, $Glu^{442} \rightarrow$ Ala, $Lys^{492} \rightarrow$ Leu, and $Lys^{515} \rightarrow$ Ala are the first *N*-domain mutants for which this characteristic is reported. The reduced rate of the $E_1PCa_2 \rightarrow E_2P$ transition could reflect a general destabilization of inter- or intra-domain interaction specific to the $E_2P$ conformation. In the wild-type enzyme, the $E_1PCa_2 \rightarrow E_2P$ transition seems to lead to tight and specific interaction of the conserved $^{181}$TGES motif of domain *A* with the phosphorylation site, thereby changing the interactions of domain *N* (1, 50). A glutaraldehyde cross-link between $Lys^{492}$ and $Arg^{678}$, tying the *N* and *P* domains together, prevents this docking of domain *A* in domain *P* (43). The recently published crystal structure of the $Ca^{2+}$-ATPase dephosphoenzyme in $E_2$ form with bound thapsigargin (51) shows that the end of the $^{441}$TETAL helix is only 7 Å away from the glutamate of the $^{181}$TGES motif of domain *A*, and a further approach might be expected in $E_2P$. Alteration to the structure of domain *N* induced by the mutations could conceivably interfere with the change of its interaction with domain *P* and domain *A* in relation to the $E_1PCa_2 \rightarrow E_2P$ transition and, possibly, also with the docking of domain *A* in domain *P*. For $Glu^{442} \rightarrow$ Ala and $Lys^{515} \rightarrow$ Ala, disruption of the $Glu^{442}$–$Lys^{515}$ salt link may be an important contributing factor, whereas $Thr^{441} \rightarrow$ Ala might affect more directly the position of the $^{441}$TETAL helix. Moreover, a defective $Mg^{2+}$ coordination, as suggested above for $Thr^{441} \rightarrow$ Ala, could contribute to the inhibition of the $E_1PCa_2 \rightarrow E_2P$ transition, as a normal rate of this step seems to require the binding of $Mg^{2+}$ (52).

For $Glu^{442} \rightarrow$ Ala, $Lys^{492} \rightarrow$ Leu, $Lys^{515} \rightarrow$ Ala, and $Arg^{560} \rightarrow$ Glu, we also observed a significant enhancement of the hydrolysis of $E_2P$ (Fig. 9 and Table II). The location of $Arg^{560}$ rather close to domain *P* is likely important for the effect of the $Arg^{560} \rightarrow$ Glu mutation on the hydrolysis of $E_2P$, as well as for the increased true affinity for $P_i$ ($K_D$) or increased rate of phosphorylation from $P_i$ ($k_2$) deduced for the $Arg^{560}$ mutants on the basis of the $E_2P$ hydrolysis rate in conjunction with apparent $P_i$ affinity (see "Results"). For the mutants with a slowed $E_1PCa_2 \rightarrow E_2P$ transition, the enhanced hydrolysis of $E_2P$ may on the other hand result from the more general destabilization of the $E_2P$ conformation discussed above.

In addition to being the phosphorylating substrate, MgATP and/or ATP exert modulatory effects on various steps of the pump cycle (*boxed ATP* in Scheme 1). Hence, in the wild-type $Ca^{2+}$-ATPase, the MgATP dependence of ATPase activity exhibits at least three activation phases, corresponding to high affinity (0–10 $\mu$M), intermediate affinity (10–200 $\mu$M), and low affinity (>200 $\mu$M). The high affinity phase reflects MgATP binding to the $E_1Ca_2$ form as phosphorylating substrate. The low affinity activation phase reflects a modulatory effect of nucleotide on the $E_1PCa_2 \rightarrow E_2P$ transition (13, 15, 16), whereas the intermediate phase most likely is due to modulation of the $Ca^{2+}$-binding $E_2 \rightarrow E_1Ca_2$ conformational transition

of the dephosphoenzyme (10, 26, 53, 54), *cf.* Scheme 1. In addition, ATP in the submillimolar concentration range enhances $E_2P$ hydrolysis (9, 12, 14). There is evidence that the latter effect is exerted only by free ATP and not MgATP (14), which implies a rather low apparent affinity in the presence of $Mg^{2+}$. Furthermore, $E_2P$ hydrolysis is so rapid in the wild type, at pH values close to neutral and in the presence of $K^+$, that it only contributes to rate limitation of the overall reaction at MgATP concentrations where the modulatory effect on the $E_1PCa_2 \rightarrow E_2P$ transition is fully implemented (13). In a titration curve such as that shown in Fig. 3, the modulatory effect on $E_2P$ hydrolysis should, therefore, be apparent only for the highest MgATP concentrations. A subject of much controversy is the question whether the phosphorylating and modulatory MgATP/ATP molecules are at the same locus, exhibiting variable affinity during the transport cycle depending on conformational state, or a separate low affinity allosteric site exists on the same $Ca^{2+}$-ATPase polypeptide chain (14, 29, 55–58). A similar discussion exists for the closely related $Na^+$,$K^+$-ATPase, although in this case it seems that only the $E_2(K_2) \rightarrow E_1(Na_3)$ transition and not phosphoenzyme processing is modulated by nucleotide (59–62).

To the extent it could be studied, the intermediate activation phase, reflecting modulation of the $E_2 \rightarrow E_1Ca_2$ conformational transition of the unphosphorylated $Ca^{2+}$-ATPase, seemed less pronounced or right-shifted in the mutants that showed reduced MgATP binding affinity at the substrate site (Fig. 3), consistent with the evidence that only one site per polypeptide chain is available for binding of nucleotide within the high and intermediate affinity ranges (14, 29). On the other hand, mutants $Arg^{560} \rightarrow$ Leu, $Arg^{560} \rightarrow$ Val, $Leu^{562} \rightarrow$ Phe, $Thr^{441} \rightarrow$ Ala, $Glu^{442} \rightarrow$ Ala, and $Lys^{515} \rightarrow$ Ala all showed a distinct low affinity modulatory effect of nucleotide on the overall ATPase reaction and on the rate-limiting $E_1PCa_2 \rightarrow E_2P$ transition, as well as a modulatory effect on the hydrolysis of $E_2P$, despite the fact that a conspicuous lowering of nucleotide affinity was seen for the substrate site of the dephosphoenzyme in these mutants, as discussed above. There was no evidence for a significant lowering of the apparent affinity with which MgATP or ATP modulates the $E_1PCa_2 \rightarrow E_2P$ transition in any of these mutants, as the increase of MgATP concentration from 1 to 5 mM induced a wild type-like 2-fold enhancement in all cases (Fig. 7 and Table II). The tendency for the ATPase activity of $Thr^{441} \rightarrow$ Ala, $Glu^{442} \rightarrow$ Ala, and $Lys^{515} \rightarrow$ Ala to level off more abruptly than that of the wild type at the highest MgATP concentrations (Fig. 3) is likely due to the very strong rate limitation by the $E_1PCa_2 \rightarrow E_2P$ transition in these mutants, which prevents the ATP modulation of $E_2P$ hydrolysis from contributing significantly to the overall activity, because $E_2P$ hydrolysis is already much faster than the $E_1PCa_2 \rightarrow E_2P$ transition without ATP modulation. When the nucleotide dependence of phosphoenzyme processing was examined for the mutants with alterations to $Phe^{487}$, $Arg^{489}$, and $Lys^{492}$ (Table II), we also found a significant modulatory effect, although slightly less pronounced than for wild type. Hence, our results seem to imply that none of the residues studied here are critical to the ligation of modulatory nucleotide in the phosphoenzyme. It is interesting to note the resemblance of the MgATP dependences of ATPase activity of the mutants to data obtained for wild type by titration with MgATP deoxy analogues lacking the 2′- or 3′-hydroxyl group on the ribose (63). Also, in these cases, the affinities corresponding to the substrate site of the dephosphoenzyme were lowered, whereas the activation phase above 200 μM was virtually unaltered (63). These data, as well as our results, seem to support the hypothesis that the modulatory site on the phosphoenzyme differs substantially from the substrate site. On the other hand, the "plasticity" exhibited by the substrate site, as seen by the dependence of the mutational effects on the nucleotide studied, calls for some caution of interpretation. We have discussed above that ATP may bind differently from MgATP. Furthermore, it is noteworthy that TNP-$8N_3$-MgATP can function as a substrate supporting efficient $Ca^{2+}$ transport and is hydrolyzed even when tethered at $Lys^{492}$ (64), although the data in Table I clearly indicate that TNP-$8N_3$-MgATP is not bound exactly as MgATP. Thus, the adenosine portion of the substrate may not need to occupy a very precise locus, and the same could be even more applicable to the modulatory nucleotide bound with low affinity. It is possible that the modulation of the kinetics of the conformational change and hydrolysis of the phosphoenzyme arise primarily from electrostatic interaction between the covalently attached phosphoryl group and the phosphates of the modulatory ATP. The principal requirement might, thus, be that the γ-phosphate or β- and γ-phosphates is/are near the phosphoryl group covalently attached at $Asp^{351}$. This notion is supported by the finding that ATP, AMP($CH_2$)PP, or $PP_i$, but not ADP or $P_i$, exert modulatory effects on ATPase activity (65). Because ATP and not MgATP seems to bind to $E_2P$, which contains $Mg^{2+}$ tightly bound together with the covalently attached phosphoryl group (14), it may be speculated that one of the major interactions responsible for the low affinity binding of nucleotide to the phosphoenzyme occurs between ATP and the $Mg^{2+}$ already bound. In this scenario, there may not be very specific requirements for amino acid side chains in domain *N* to ligate the adenosine part of the modulatory nucleotide. At the moment this seems an attractive working hypothesis as an alternative to invoking a second site at a location completely distinct from that of the substrate site.

*Acknowledgments*—We thank Lene Jacobsen, Karin Kracht (Aarhus, Denmark), and Irene Mardarowicz (Cape Town, South Africa) for expert technical assistance. We also thank Dr. R. J. Kaufmann (Genetics Institute, Boston) for the gift of the expression vector pMT2.

REFERENCES

1. Toyoshima, C., Nakasako, M., Nomura, H., and Ogawa, H. (2000) *Nature* **405,** 647–655
2. Pick, U., and Bassilian, S. (1981) *FEBS Lett.* **123,** 127–130
3. Mitchinson, C., Wilderspin, A. F., Trinnaman, B. J., and Green, N. M. (1982) *FEBS Lett.* **146,** 87–91
4. McIntosh, D. B., Woolley, D. G., and Berman, M. C. (1992) *J. Biol. Chem.* **267,** 5301–5309
5. McIntosh, D. B., Woolley, D. G., Vilsen, B., and Andersen, J. P. (1996) *J. Biol. Chem.* **271,** 25778–25789
6. Nakamoto, R. K., and Inesi, G. (1984) *J. Biol. Chem.* **259,** 2961–2970
7. DeJesus, F., Girardet, J., and Dupont, Y. (1993) *FEBS Lett.* **332,** 229–232
8. Verjovski-Almeida, S., and Inesi, G. (1979) *J. Biol. Chem.* **254,** 18–21
9. Shigekawa, M., and Dougherty, J. P. (1978) *J. Biol. Chem.* **253,** 1451–1457
10. Scofano, H. M., Vieyra, A., and de Meis, L. (1979) *J. Biol. Chem.* **254,** 10227–10231
11. Møller, J. V., Lind, K. E., and Andersen, J. P. (1980) *J. Biol. Chem.* **255,** 1912–1920
12. McIntosh, D. B., and Boyer, P. D. (1983) *Biochemistry* **22,** 2867–2875
13. Champeil, P., le Maire, M., Andersen, J. P., Guillain, F., Gingold, M., Lund, S., and Møller, J. V. (1986) *J. Biol. Chem.* **261,** 16372–16384
14. Champeil, P., Riollet, S., Owlowski, S., Guillain, F., Seebregts, C. J., and McIntosh, D. B. (1988) *J. Biol. Chem.* **263,** 12288–12294
15. Wakabayashi, S., Oguruso, T., and Shigekawa, M. (1986) *J. Biol. Chem.* **261,** 9762–9769
16. Bodley, A. L., and Jencks, W. P. (1987) *J. Biol. Chem.* **262,** 13997–14004
17. Axelsen, K. B., and Palmgren, M. G. (1998) *J. Mol. Evol.* **46,** 84–101
18. Abu-Abed, M., Tapas, K. M., Kainosho, M., MacLennan, D. H., and Ikura, M. (2002) *Biochemistry* **41,** 1156–1164
19. Maruyama, K., and MacLennan, D. H. (1988) *Proc. Natl. Acad. Sci. U. S. A.* **85,** 3314–3318
20. Maruyama, K., Clarke, D. M., Fujii, J., Inesi, G., Loo, T. W., and MacLennan, D. H. (1989) *J. Biol. Chem.* **264,** 13038–13042
21. Hua, S., Ma, H., Lewis, D., Inesi, G., and Toyoshima, C. (2002) *Biochemistry* **41,** 2264–2272
22. Vilsen, B., Andersen, J. P., Clarke, D. M., and MacLennan, D. H. (1989) *J. Biol. Chem.* **264,** 21024–21030
23. Kaufman, R. J., Davies, M. V., Pathak, V. K., and Hershey, J. W. (1989) *Mol. Cell. Biol.* **9,** 946–958
24. Chen, C., and Okayama, H. (1987) *Mol. Cell. Biol.* **7,** 2745–2752
25. Vilsen, B., Andersen, J. P., and MacLennan, D. H. (1991) *J. Biol. Chem.* **266,** 16157–16164

26. Sørensen, T., Vilsen, B., and Andersen, J. P. (1997) *J. Biol. Chem.* **272,** 30244–30253
27. Sørensen, T. L., Dupont, Y., Vilsen, B., and Andersen, J. P. (2000) *J. Biol. Chem.* **275,** 5400–5408
28. Andersen, J. P., Vilsen, B., Leberer, E., and MacLennan, D. H. (1989) *J. Biol. Chem.* **264,** 21018–21023
29. Seebregts, C. J., and McIntosh, D. B. (1989) *J. Biol. Chem.* **264,** 2043–2052
30. Vilsen, B., and Andersen, J. P. (1992) *J. Biol. Chem.* **267,** 25739–25743
31. Bers, D. M., Patton, C. W., and Nuccitelli, R. (1994) *Methods Cell Biol.* **40,** 3–29
32. Vianna, A. L. (1975) *Biochim. Biophys. Acta* **410,** 389–406
33. McIntosh, D. B., Woolley, D. G., MacLennan, D. H., Vilsen, B., and Andersen, J. P. (1999) *J. Biol. Chem.* **274,** 25227–25236
34. Clausen J. D., McIntosh D. B., Woolley D. G., and Andersen J. P. (2001) *J. Biol. Chem.* **276,** 35741–35750
35. Vilsen, B., and Andersen, J. P. (1992) *J. Biol. Chem.* **267,** 3539–3550
36. Murphy, A. J. (1988) *Biochim. Biophys. Acta* **946,** 57–65
37. Murphy, A. J. (1978) *J. Biol. Chem.* **253,** 385–389
38. Petithory, J. R., and Jencks, W. P. (1986) *Biochemistry* **25,** 4493–4497
39. Stefanova, H. I., East, J. M., Gore, M. G., and Lee, A. G. (1992) *Biochemistry* **31,** 6023–6031
40. Suzuki, S., Obara, M., Kuwayama, H., and Kanazawa, T. (1987) *J. Biol. Chem.* **262,** 15448–15456
41. Hua, S., Inesi, G., Nomura, H., and Toyoshima, C. (2002) *Biochemistry* **41,** 11405–11410
42. Patchornik, G., Munson, K., Goldshleger, R., Shainskaya, A., Sachs, G., and Karlish, S. J. D. *Biochemistry* **41,** 11740–11749
43. McIntosh, D. B. (1992) *J. Biol. Chem.* **267,** 22328–22335
44. Zhang, P., Toyoshima, C., Yonekura, K., Green, N. M., and Stokes, D. L. (1998) *Nature* **392,** 835–839
45. Jacobsen, M. D., Pedersen, P. A., and Jorgensen, P. L. (2002) *Biochemistry* **41,** 1451–1456
46. Honig, B. H., and Hubbell, W. L. (1984) *Proc. Natl. Acad. Sci. U. S. A.* **81,** 5412–5416
47. Vilsen, B., Andersen, J. P., and MacLennan, D. H. (1991) *J. Biol. Chem.* **266,** 18839–18845
48. Clarke, D. M., Loo, T. W., and MacLennan, D. H. (1990) *J. Biol. Chem.* **265,** 22223–22227
49. Clarke, D. M., Loo, T. W., and MacLennan, D. H. (1990) *J. Biol. Chem.* **265,** 14088–14092
50. Danko, S., Yamasaki, K., Daiho, T., Suzuki, H., and Toyoshima, C. (2001) *FEBS Lett.* **505,** 129–135
51. Toyoshima, C., and Nomura, H. (2002) *Nature* **418,** 605–611
52. Wakabayashi, S., and Shigekawa, M. (1987) *J. Biol. Chem.* **262,** 11524–11531
53. Stahl, N., and Jencks, W. P. (1984) *Biochemistry* **23,** 5389–5392
54. Wakabayashi, S., and Shigekawa, M. (1990) *Biochemistry* **29,** 7309–7318
55. Coll, R. J., and Murphy, A. J. (1991) *Biochemistry* **30,** 1456–1461
56. Bishop, J. E., Al Shawi, M. K., and Inesi, G. (1987) *J. Biol. Chem.* **262,** 4658–4663
57. Cable, M. B., Feher, J. J., and Briggs, F. N. (1985) *Biochemistry* **24,** 5612–5619
58. Stokes, D. L., and Green, N. M. (2000) *Biophys. J.* **78,** 1765–1776
59. Moczydlowski, E. G., and Fortes, P. A. (1981) *J. Biol. Chem.* **256,** 2357–2366
60. Scheiner-Bobis, G., Antonipillai, J., and Farley, A. R. (1993) *Biochemistry* **32,** 9592–9599
61. Ward, D. G., and Cavieres, J. D. (1988) *J. Biol. Chem.* **273,** 33759–33765
62. Teramachi, S., Imagawa, T., Kaya, S., and Taniguchi, K. (2002) *J. Biol. Chem.* **277,** 37394–37400
63. Coan, C., Amaral, J. A., Jr., and Verjovski-Almeida, S. (1993) *J. Biol. Chem.* **268,** 6917–6924
64. McIntosh, D. B., and Woolley, D. G. (1994) *J. Biol. Chem.* **269,** 21587–21595
65. Dupont, Y. (1977) *Eur. J. Biochem.* **72,** 185–190

# Importance of Conserved N-domain Residues Thr$^{441}$, Glu$^{442}$, Lys$^{515}$, Arg$^{560}$, and Leu $^{562}$ of Sarcoplasmic Reticulum $Ca^{2+}$-ATPase for MgATP Binding and Subsequent Catalytic Steps: PLASTICITY OF THE NUCLEOTIDE-BINDING SITE

Johannes D. Clausen, David B. McIntosh, Bente Vilsen, David G. Woolley and Jens Peter Andersen

*J. Biol. Chem. 2003, 278:20245-20258.*
*doi: 10.1074/jbc.M301122200 originally published online March 20, 2003*

---